



Universiteit
Leiden
The Netherlands

Lipidomics study in liver metabolic diseases

Singh, M.

Citation

Singh, M. (2024, June 13). *Lipidomics study in liver metabolic diseases*. Retrieved from <https://hdl.handle.net/1887/3762800>

Version: Publisher's Version

License: [Licence agreement concerning inclusion of doctoral thesis in the Institutional Repository of the University of Leiden](#)

Downloaded from: <https://hdl.handle.net/1887/3762800>

Note: To cite this publication please use the final published version (if applicable).

Chapter 6

An old new player in MCADD: reduced free coenzyme A availability in medium-chain acyl-CoA dehydrogenase deficiency

(To be revised according to manuscript in preparation)

Christoff Odendaal*, Ligia Akemi Kiyuna*, **Madhulika Singh***, Albert Gerding, Miriam Langelaar-Makkinje, Marianne van der Zwaag, Asmara Drachman, Vladimíra Cetková, Gaby Liem Foeng Kioen, Anne-Claire M.F. Martines, Nicolette C. A. Huijkman, Hein Schepers, Bart van de Sluis, Dirk-Jan Reijngoud, Ody C.M. Sibon, Amy C. Harms, Thomas Hankemeier, Barbara M. Bakker

*authors contributed equally

Abstract

Background: Medium-chain acyl-CoA dehydrogenase deficiency (MCADD) is the most prevalent mitochondrial fatty-acid oxidation (mFAO) disorder. Among its symptoms, life-threatening hypoketotic hypoglycemia remains poorly understood. Using a computational model of hepatic mFAO, we predicted that MCADD leads to an increased risk of free coenzyme A (CoASH) depletion due to sequestration into medium-chain acyl-CoA esters, which may in turn impact glucose production. Therefore, we aimed to quantify the acyl-CoA esters and the CoA pool in MCAD-deficient cells and mouse liver. Moreover, we investigated the existence of compensatory mechanisms that would respond to such CoA sequestration.

Methods: Free CoA, acyl-CoA and acylcarnitine profiles were measured in wildtype (WT) and MCAD knockout (KO) HepG2 cells. $^{13}\text{C}_3^{15}\text{N}_1$ -labeled pantothenate (precursor of free CoA) was used to estimate the CoA synthesis rate. Total CoA (sum of the free CoA fraction and CoA thioesters) and the expression of proteins involved in CoA turnover were analyzed in HepG2 cells as well as in the liver of WT & MCAD KO mice (C57BL/6, exposed to 14 h overnight fasting at room temperature followed by 4 h fasting at 4 °C).

Results: Compared to WT, MCAD-KO cells presented increased levels of C6-C10 acyl-CoAs, and reduced levels of free CoA, short- and long-chain acyl-CoAs. The changes in the acyl-CoA profile were mirrored in the cognate acylcarnitines. Under cold exposure, hepatic total CoA was strongly increased in MCAD-KO mice compared to the WT group, coinciding with an upregulation of acyl-CoA thioesterases (ACOTs), carnitine acyltransferases and pantothenate kinases. Computational simulations predicted recovery of free CoA and reduction in C8-CoA accumulation in the MCAD-KO model on increasing total CoA and ACOT levels simultaneously.

Discussion: Validating the computational simulations, free CoA was reduced in MCAD-KO cells due to its sequestration into medium-chain acyl-CoAs. Altogether, the experimental and modelling results suggest the role of multiple compensatory mechanisms in MCAD deficiency, specifically the upregulation of CoA biosynthesis and ACOT expression, which would work towards increasing the free CoA fraction and relieving the accumulation of acyl-CoA species, respectively.

Keywords

MCADD; *in silico*; *in vitro*; *in vivo*; Acyl-CoA esters; Total CoA; Free CoA/CoASH

1. Introduction

Coenzyme A (CoA) is vital for many metabolic pathways, particularly in the mitochondria. The most recent genome-scale reconstruction of human metabolism, Human1, contained 1044 reactions that consume or produce CoA – 8% of all its reactions [1]. It is essential for the mitochondrial fatty acid oxidation (mFAO), the oxidation of branched-chain amino acids and the tricarboxylic acid cycle, among others. Classically, symptoms of a metabolic disease are attributed to the function of the pathway in which a defect is found. For instance, an impairment of the mFAO limits the availability of energy from fat. It has been hypothesized, however, that a range of diseases in which CoA is implicated might also exert their pathogenicity via the accumulation of metabolites bound to CoA (acyl-CoA esters) and the consequent depletion of the free form of CoA (free CoA, also referred as CoASH). This hypothesis has been called CASTOR for Coenzyme A Sequestration, Toxicity and Redistribution [2–4]. Common symptoms of CASTOR diseases include acidosis, hypoglycemia and hyperammonemia, often with liver, heart or multiple organ dysfunction. These common symptoms are attributed to a lack of CoA required for gluconeogenesis and oxidative phosphorylation, as well as ureagenesis [2,5].

Medium-chain acyl-CoA dehydrogenase deficiency (MCADD, #OMIM 201450) is the most prevalent inborn error of mitochondrial fatty acid oxidation [6]. In humans, the medium-chain acyl-CoA dehydrogenase (MCAD) enzyme catalyzes the conversion of acyl-CoA esters with a chain length of 6-12 carbons into the corresponding enoyl-CoA esters. It is considered the most important enzyme for the oxidation of medium-chain fatty acids. Around 80% of clinically presenting patients are homozygous for the c.985A>G missense mutation in the *ACADM* gene, with less than 1% residual MCAD activity [7,8]. In blood and serum of patients, elevated levels of acylcarnitine esters of 6-10 carbon-atom chain length are observed, as well as an elevated ratio of C8/10 acylcarnitines [7]. These are thought to correspond to elevated levels of the corresponding acyl-CoA esters in the liver [9,10]. Before MCADD was included in the newborn screening programmes of many countries [11–14], it was typically diagnosed through life-threatening hypoketotic hypoglycemia in the first five years of life, or via a symptomatic sibling [15–17]. This hypoglycemia in combination with the accumulation of medium-chain acyl-CoA esters would make MCADD a typical CASTOR disease [2].

Direct evidence for accumulation of CoA esters and depletion of free CoA in putative CASTOR diseases is limited [3,4,18]. Most often the cognate carnitine esters are measured [3,4]. Propionyl-CoA carboxylase deficiency (propionic acidemia) is an example of

mitochondrial disorder resulting in reduced metabolism of propionyl-CoA. Like other CASTOR diseases, propionic acidemia is associated with metabolic acidosis, hypoglycemia, and hyperammonemia [19]. A study conducted measurements of both CoA and carnitine metabolites and demonstrated an elevated level of propionyl carnitine, propionyl-CoA and reduced free CoA in mouse model of these disorders [20,21]. Furthermore, this study also revealed that the metabolite concentration of free CoA can be restored by pharmacological activation of CoA biosynthesis [20]. A further piece of theoretical evidence of CoA metabolism comes from computational models of the mitochondrial fatty-acid oxidation in rodents. Model simulations predicted that the loss of MCAD activity causes severe reduction of free CoA due to its sequestration into medium-chain acyl-CoAs [22,23]. The simulations suggest that the mFAO pathway is particularly vulnerable to the CASTOR phenotype, due to the promiscuity of mFAO enzymes for substrates of different acyl-chain lengths, which may lead to a vicious cycle of acyl-CoA accumulation and free CoA depletion [24].

Quantitative and simultaneous analysis of acyl-CoA esters and free CoA is challenging due to the technical difficulty associated with the measurement of these compounds such as use of multiple methods for covering short-to long-chain species (high to low polarity) [25]. Recently, hydrophilic interaction liquid chromatography coupled with tandem mass spectrometry (HILIC-MS/MS) was shown to achieve a comprehensive analysis of free CoA and short- to long-chain acyl-CoA (covering carbon chain lengths from 2 to 18) in a single analytical run with good linearity, precision, and recovery [26]. This method allowed to explore the CASTOR hypothesis in MCADD experimentally in a convenient and direct way.

The levels of free CoA are not solely regulated by sequestration into CoA esters. Free CoA sequestration may be relieved by hydrolysis via thioesterases [27] or conversion into the cognate carnitine esters by acyltransferases [28–30]. Additionally, CoA can be synthesized *de novo* from pantothenate (vitamin B5) [31]. The biosynthesis of CoA may be inhibited by high levels of acyl-CoA species. Pantothenate kinase (PANK) is the first enzyme of CoA synthesis from pantothenate. Particularly, the hepatic PANK3 is inhibited by medium-chain acyl-CoA species. Last but not least, local free CoA levels may be affected by rerouting of acyl-CoA into the peroxisomal beta-oxidation [32]. The ability to redistribute CoA across the organelles has been proposed, for instance by purported peroxisomal CoA carrier SLC25A17 [33], and its mitochondrial cognates SLC25A16 [34] and SLC25A42 [35]. It is well known that this surrounding metabolic network (**Figure 1A**) of CoA release, biosynthesis and redistribution is regulated by gene expression in response to feeding/fasting cycles [36,37], cold [38] and

pharmacological intervention (e.g. HoPan) [29]. It is not known, however, how the network is regulated in response to CASTOR diseases, such as MCADD.

Addressing the overarching question of how free and total CoA are impacted by MCADD, the present study used *in silico*, *in vitro* and *in vivo* models. In agreement with previous reports, the *in silico* model of human liver (**Figure 1B**) suggests that an accumulation in C8-CoA dominates the CoA pool in mitochondria in MCADD conditions [22,23], which was experimentally tested in *in vitro* (wildtype (WT) and MCAD-knockout (KO) HepG2 cells) using the recently developed HILIC-MS/MS method [26]. Stable isotope labelling which could be detected by the HILIC-MS/MS method, was employed to track any possible changes in CoA synthesis in WT and MCAD-KO conditions. Similar experiments were performed in *in vivo* (WT and MCAD-KO mice liver) under physiologically relevant conditions. Gene expression levels involved in CoA turnover were also analyzed both *in vitro* and *in vivo*. Taken together, our study shows how multi-scale experimental and computational tools can be used to untangle systemic changes in MCADD.

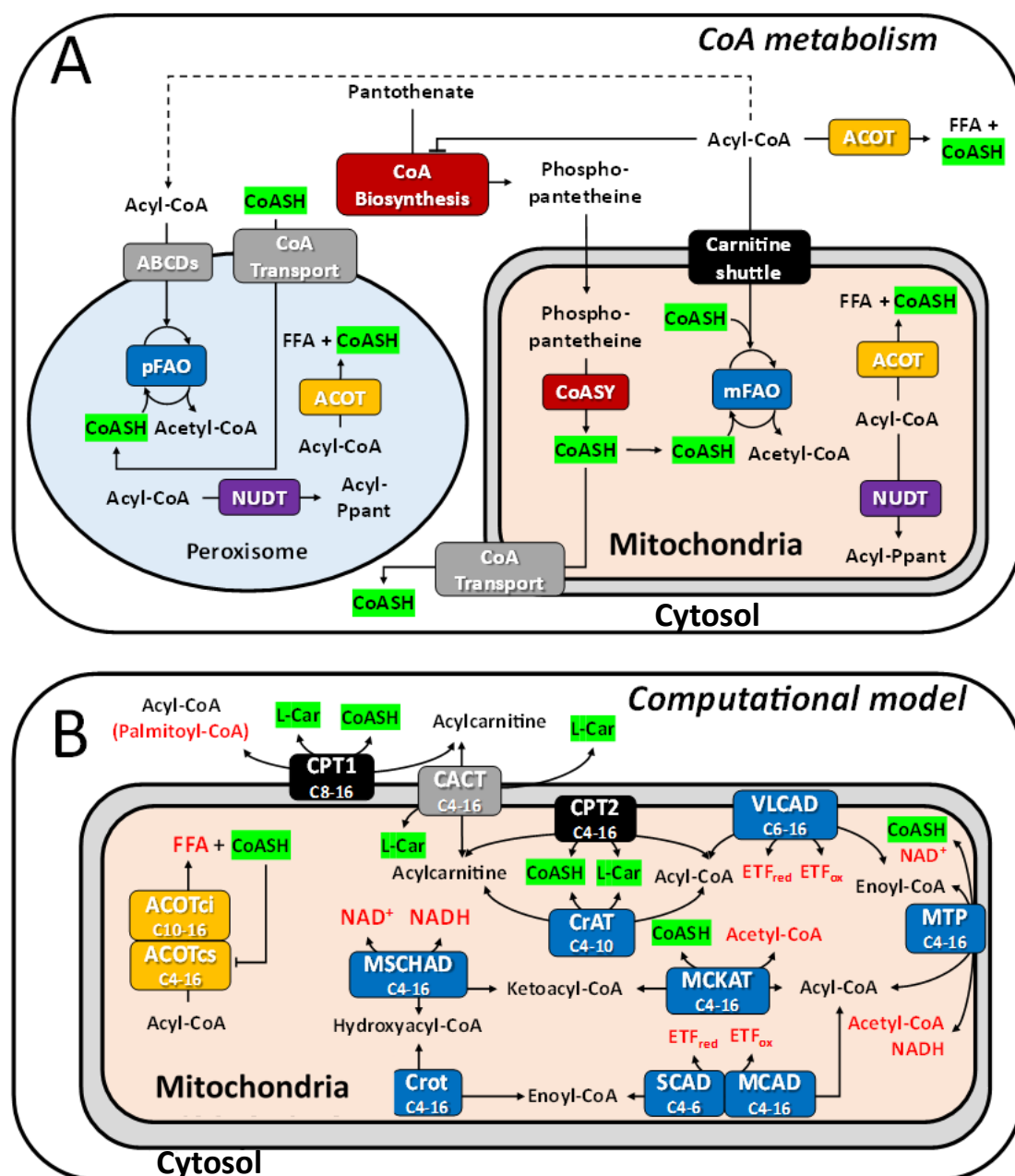


Figure 1. Coenzyme A compartmentalization, synthesis and sequestration. Boxes indicate pathways or individual enzymes: carnitine acyltransferases in black, transporters in grey, thioesterases in yellow, nudix hydrolases in purple, fatty acid oxidation in blue and CoA biosynthesis in red. Metabolites are in black text. CoASH and L-Car (highlighted green) represent free CoA and L-carnitine, respectively. **A.** Pathways investigated in this study span three compartments: the cytosol, mitochondrion, and peroxisome. pFAO = peroxisomal fatty acid oxidation, CoASY = bifunctional CoA synthase, ABCD = ATP-binding cassette domain transporter, NUDT = nudix hydrolase (nucleoside diphosphate linked moiety X-type motif), FFA = free fatty acid.; **B.** Reactions included in the kinetic computational model of human liver mFAO. Red metabolites have fixed concentrations in the model. Subscript indicates the chain-length specificity of each of the reactions. CPT1/2 = carnitine palmitoyltransferase 1/2, CACT = carnitine acylcarnitine translocase, CrAT = carnitine acetyltransferase, VLCAD/MCAD/SCAD = very long-/medium-/short-chain acyl-CoA dehydrogenase, MTP = mitochondrial trifunctional protein, Crot = crotonase, MSCHAD = medium- and short-chain hydroxyacyl-CoA dehydrogenase, MCKAT = medium-chain ketoacyl-CoA thiolase, ACOTci/cs = CoASH-insensitive/-sensitive ACOT, ETF_{red}/ox = reduced/oxidised electron-transferring flavoprotein.

2. Materials and Methods

2.1 Chemicals and reagents

Liquid chromatography-mass spectrometry (LC-MS) grade solvents, namely acetonitrile, methanol, isopropanol and chloroform, were procured from BioSolve BV (Valkenswaard, The Netherlands). Ammonium acetate ($\geq 99\%$), was purchased from Sigma-Aldrich (St. Louis, MO, USA). Purified water was obtained through the Milli-QR Advantage A10 Water Purification System from Merck Millipore (Billerica, MA, USA). Formic acid ($>98\%$) was bought from Acros Organics (Geel, Belgium). Pentadecanoyl-CoA (C15:0-CoA) and heptadecanoyl-CoA (C17:0-CoA) in ammonium salt form were purchased from Avanti Polar Lipids (Alabaster, AL, USA). Acetyl-1,2- $^{13}\text{C}_2$ -CoA (C2:0($^{13}\text{C}_2$)-CoA) and n-heptanoyl-CoA (C7:0-CoA) as lithium salts were obtained from Sigma-Aldrich (St. Louis, MO, USA). Acylcarnitines deuterium labeled standards, L-carnitine- d_3 , propionyl-L-carnitine- d_3 , butyryl-L-carnitine- d_3 , octanoyl-L-carnitine- d_3 and octadecanoyl-L-carnitine- d_3 as hydrochloride salts were purchased from CDN Isotopes (Pointe-Claire, QC, Canada). Fetal bovine serum (FBS) and phosphate-buffered saline (PBS) were purchased from Gibco. Dulbecco's Modified Eagle Medium (DMEM) was purchased from PAN BiotechTM. L-carnitine (Product No. C0283), palmitate (Product No. P9767) and labeled pantothenate ($^{13}\text{C}_3$ - $^{15}\text{N}_1$ -pantothenate, Product No. 705837) were obtained from Sigma-Aldrich.

2.2 Computational modelling

The human liver computational model was developed by adapting a previous model of mFAO in rat liver [10]. The kinetic constants were adjusted to align with human parameters, and enzymes crucial for CoA metabolism, such as carnitine acetyl-CoA transferase and acyl-CoA thioesterase, were incorporated. In this model, metabolites were distributed based on their solubility between the mitochondrial matrix and the inner membrane. Detailed modeling conditions can be found in previous publication [23], and the complete model is accessible on the JWS Online Biological Systems Modelling repository [39]. It can be viewed, downloaded, and simulated directly through JWS Online [40].

2.3 Cell lines

HepG2 cells, wildtype (WT) and MCAD-knockout (KO), were used for all *in vitro* experiments. In each individual experiment, WT and 3 MCAD-KO clones (3 biological replicates- KO4, KO9, KO21) were tested in parallel. The cell lines, their generation and validation of the knockout are described in detail elsewhere [23].

2.4 *In vitro* experiments

HepG2 cells were cultured in maintenance medium (**Table 1**), unless stated otherwise, and kept at 37 °C and 5% CO₂. For the experiments, 2-4 x10⁶ cells were seeded in 100 mm plates and kept for 24-48 h in maintenance medium until reaching ~70% confluency. On the day of the experiment, cells were washed 2 times with PBS, and the maintenance medium was replaced by the condition medium: *high-fat low-glucose medium* or *high-fat no-glucose medium* (**Table 1**). After 24 h, the cells were washed twice with ice-cold PBS. Then, 200 µL of ice-cold MeOH was added and the adherent cells were further scraped from the plates using a pipet tip and transferred to a tube. The samples were divided into two equal parts of 100 µL each. Samples were immediately frozen at -80 °C until further analysis. One part was used for LC-MS analysis, while the other was used for protein quantification. These samples were used for free CoA, acyl-CoA esters and acylcarnitine analysis. Protein was quantified using the BCA assay (Thermo Scientific, 23225).

For label incorporation experiments, *high-fat low-glucose medium* (**Table 1**) was made using pantothenate free DMEM (PAN Biotech™) supplemented with 16 µM of ¹³C₃-¹⁵N₁-pantothenate. This was equal to the unlabeled pantothenate concentration in the maintenance media. Moreover, dialysed FBS (Fisher scientific, Product Code 11521841) was used instead of normal FBS. The remaining steps in the procedure were same as described above. These samples were used for the analysis of free CoA and labeled free CoA.

Table 1. Composition of the media used for *in vitro* experiments.

Medium components	Maintenance	high-fat low-glucose	high-fat no-glucose
DMEM	P04-01500	P04-01500	P04-01548S1
FBS	10%	10%	10%
Glucose	1.0 g L ⁻¹	1.0 g L ⁻¹	-
Pyruvate	1 mM	1 mM	-
Glutamine	3 mM	3 mM	-
L-Carnitine	-	2 mM	2 mM
BSA-bound Palmitate	-	0.5 mM	0.5 mM

A different protocol, described by Srinivasan et al. [41] has been used for the analysis of total CoA (sum of the free CoA fraction and acyl-CoA thioesters). HepG2 cells were incubated in *high-fat low-glucose medium* supplemented with ¹³C₃-¹⁵N₁-pantothenate (16 µM) for 24 h. The cells kept in the maintenance medium (**Table 1**) were used as control (0 h). The cells were collected in ice-cold medium and washed twice in ice-cold PBS. The pellet was reconstituted in 600 µL MilliQ H₂O and the lysate was sonicated using a Sonics Vibra cell VCX130 (25 sec, 50% amplitude, 2 times). Lysates were centrifuged at 14000 rpm for 15 min at 4 °C. In a new

tube, 80 μ L Tris (2-carboxyethyl)phosphine hydrochloride (10 mM) was added to 400 μ L supernatant and incubated for 15 min at room temperature. Next, samples were spun down (14000 rpm, 15 min, 4 °C). In a new tube, 40 μ L ammonia solution (12.5% v/v) was added to 400 μ L supernatant and incubated while shaking at 500 rpm at 60°C for 60 min. Lastly, samples were dried using a SpeedVac (Eppendorf) and reconstituted in 100 μ L ice-cold methanol. These samples were further extracted and analyzed for total CoA and labeled total CoA analysis using the previously reported LC-MS/MS method [26].

For all *in vitro* experiments, we had 5 technical replicates (5 plates per condition). We conducted each experiment at least three times. In total, for each cell line, 15-18 separate cell cultures were assayed in 3-4 rounds of measurements.

Further details about MCAD overexpression in MCAD-KO HepG2 cells, protein extraction and immunoblotting have been mentioned in **Supplementary information**.

2.5 Acyl-CoA and acylcarnitine extraction from HepG2 cells and LC-MS/MS analysis

Sample preparation was performed using protocol based on Bligh and Dyer method [42]. A detailed protocol is available in **Supplementary information**.

For acyl-CoA and acylcarnitine profiling, an Acquity UPLC system from Waters (Milford, MA, USA) coupled to an AB Sciex QTRAP 6500 mass spectrometer equipped with Turbo V source (Concord, ON, Canada) was utilized. Both acyl-CoA and acylcarnitine analysis were conducted using positive electrospray ionization (ESI) in scheduled multiple reaction monitoring (sMRM) mode. The acyl-CoA profiling was performed using HILIC-MS/MS conditions according to the previously published study [26], employing a SeQuant® ZIC®-cHILIC-HPLC (100 x 2.1 mm) column, with a particle size of 3.0 μ m and a pore size of 100Å (Merck, Darmstadt, Germany). The detailed explanation is provided in **Supplementary information**.

The acylcarnitine profiling was performed using a reversed-phase liquid chromatography-tandem mass spectrometry (RPLC-MS/MS) method using the AccQ-Tag™ Ultra C18 column with dimensions of 2.1 x 100 mm and a particle size of 1.7 μ m from Waters (Milford, MA, USA). The settings and configurations are described in detail in **Supplementary information**.

2.6 *In vivo* experiments

Male MCAD-KO and wildtype (WT) littermate mice on a C57BL/6J background were kept in the housing facility under temperature 21 °C and light-controlled (12 h light) conditions, and had free access to food and drinking water. All experiments were approved by the Ethics

Committee for Animal Experiments of the University of Groningen (Netherlands). In the first experiment, 8-week old WT and MCAD-KO mice were divided in two groups: (1) fed and (2) 14 h fasted. Both groups were fed with commercially available laboratory chow diet (V1554-703, Ssniff). For the fasted group, on the day of the experiment, WT and MCAD-KO mice were transferred to a new cage without food, but with free access to water. The animals were overnight fasted for 14 h at 21 °C, and sacrificed. In a second experiment, 8-week old WT and MCAD-KO mice were exposed to a third condition, (3) 14 h fasted and cold-exposed. For condition (3), prior to the start of the experiment, at the age of 4-week, mice were fed with a chow-like semi-synthetic diet (D12450B, Research Diet Services) for 4 weeks. On the experiment day, 8 week WT and MCAD-KO mice were 14 h overnight fasted at 21 °C, then transferred to a 4 °C environment for 4 h, also fasted (total of 18 h fasting). For all the experimental conditions (1. Fed; 2. Fasted; 3. Fasted and cold-exposed), mice were terminated via cardiac puncture under isoflurane anesthesia, and the liver was collected for biochemical analysis.

The sample preparation and HPLC analysis protocol for measuring total CoA, phosphopantetheine (P-Pant) and dephospho-CoA (dPCoA) in mice samples were described in a previously reported study [41]. The details have been provided in the **Supplementary information**.

2.7 RNA extraction and quantitative real-time qPCR

RNA was isolated using the RNeasy® Plus Universal Mini Kit (Qiagen, 73404). Forward and reverse primers for human and murine genes are annotated in **Table S2 and S3**, respectively. RT-PCR was performed using FastStart Universal Sybr Green (Roche, 0413914001) on QuantStudio™ 7 (Applied Biosystems). The thermal cycling consisted of 10 min hold at 95 °C, followed by 40 cycles of 15 sec at 95 °C, 30 sec at 60 °C and 30 sec at 72 °C. The Ct values were expressed relative to YWHAZ (HepG2 cells) and 36B4 (mouse), and normalized to the expression level in the WT controls.

2.8 Statistical analysis and data representation

The results are shown as mean ± standard error of the mean (SEM). Analysis of differences between two groups were done using an unpaired Student's t-test. For the comparison of three or four groups, we performed one-way Brown-Forsythe ANOVA followed by the Dunnett's T3 posthoc test. Briefly, Brown-Forsythe ANOVA is a variation of the ordinary ANOVA, which does not assume the same standard deviations across the groups, and the Dunnett's T3

test corrects for the multiple comparisons performed against one control group. These analyses were performed using GraphPad Prism version 9.1 for Windows (GraphPad Software). The results were considered statistically significant when the p-value was smaller than 0.05.

All the mouse data are shown as mean \pm standard error of the mean (SEM). Regarding the HepG2 cells (WT, MCAD-KO4, MCAD-KO9, MCAD-KO21), the results were presented in a distinct way. For all the HepG2 analyses, (I) the experiments were repeated up to three times (independent experiments/biological repeats), (II) independent experiments consisted of 4-5 technical replicates (parallel cell cultures), and (III) the results obtained consisted of values relative to the control WT group within each experiment, instead of absolute values. In other words, assuming the control WT group to be 1, the values indicated how much the MCAD-KO cells varied (or not) in relation to the control. As a consequence, the average of the WT group across experiments was 1, which did not allow for the performance of statistical test of combined experiments due to the lack of variance in the control group. To circumvent this issue, we performed statistical analysis per experiment instead. The significance scores per experiment and per MCAD-KO clone are detailed in the supplement (**Tables S4-S7**).

3. Results

We employed *in silico*, *in vitro* and *in vivo* models to investigate the impact of MCADD on CoA metabolism. The findings from *in silico* simulations were validated through cellular (*in vitro*) and animal (*in vivo*) experiments. Additionally, gene expression analysis was conducted to observe the influence on CoA metabolism and identify potential compensatory mechanisms.

3.1 MCAD deficiency causes sequestration of CoA into medium-chain acyl-CoA esters

We first investigated how the complete deficiency of MCAD activity would affect the concentrations of free CoA and acyl-CoA esters. To this end we used a previously constructed and experimentally validated computational model [23] that simulates the oxidation of saturated, even-chain fatty acids in human liver mitochondria. The model starts from palmitoyl-CoA (a CoA ester with an acyl chain of 16 carbon atoms). It is based on detailed kinetic equations for each of the enzymes depicted in **Figure 1B**. Kinetic parameters were taken as much as possible from human enzymes and were obtained under physiological conditions. The model accurately predicts the biochemical characteristics of inherited mFAO deficiencies, including short-, medium-, and very long-chain acyl-CoA dehydrogenase deficiency (SCADD, MCADD and VLCADD). The model predicted a strong increase of the C8-CoA concentration and a lesser increase of C6-CoA (**Figure 2A**), while all other acyl-CoA ester concentrations

were significantly decreased in the MCAD-KO relative to the wildtype control (WT) (**Figure 2A**). In agreement with the CASTOR hypothesis, free CoA was decreased in the MCAD-KO relative to WT. Only acetyl-CoA (C2-CoA) was unchanged in the simulations, as it had a fixed boundary concentration in the model. The elevated C6- and C8-CoA concentrations were expected, since these compounds are the main substrates of MCAD. In contrast, the decline of long-chain acyl-CoA esters was counterintuitive: in linear metabolic pathways, accumulation of upstream metabolites is expected in response to an enzyme defect. However, mFAO is not a linear pathway. In its first step in the mitochondrial matrix, free CoA is required for the conversion of palmitoylcarnitine to palmitoyl-CoA by carnitine palmitoyltransferase 2 (CPT2) (**Figure 1B**). Therefore, if decreased, free CoA may limit the entry of substrate into the mFAO pathway, which in turn explains the observed reduction in long-chain acyl-CoA esters.

To validate the model predictions, we used a previously generated HepG2 MCAD-KO cell line [23]. The three clones (KO4, KO9, K21) had no detectable residual MCAD protein. Overexpression of the *ACADM* gene in KO9 and KO21 led to a partial complementation of the MCAD protein and reduced the C8-carnitine level, demonstrating that the phenotype was indeed caused by the MCAD mutation (**Figure S1**). Subsequently, WT and three MCAD-KO clones were incubated in a medium without glucose, pyruvate and glutamine, but in the presence of mFAO substrates palmitate and L-carnitine, condition named as *high-fat no-glucose*. Interestingly, MCAD-KO versus WT cells showed a similar pattern in the acyl-CoA levels as predicted in the simulations (**Figure 2B**). C8-CoA and the C8/C10 acyl-CoA ester ratios strongly increased in the MCAD-KO cells compared to the WT, while free CoA and C2-C4-CoAs were decreased (**Figure S2, Table S4**). Also, in agreement with the simulations, C14-CoA was reduced in the MCAD-KO relative to the WT. A more detailed analysis showed a broader range of medium-chain acyl-CoA species (C6 and C10) upregulated in the MCAD-KO cells, but not observed in the simulations (**Figure 2A and 2B**). The acylcarnitine profile (**Figure 2C**) exhibited a similar pattern as the acyl-CoA profile, with the only difference in the C12-carnitine that reduced in the MCAD-KO relative to the WT, thus mirroring the simulations even better (**Figure S3, Table S5**). We would like to emphasize that each data point in **Figure 2B and 2C** represents a different MCAD-KO clone, with at least 3 biological replicates (independent experiments), consisting of 4-5 technical replicates (parallel cell cultures).

To even further consolidate the results, the experiment was replicated in a culture medium which not only contain mFAO substrates (palmitate and L-carnitine), but also glucose, pyruvate and glutamine were present (named *high-fat low-glucose*), with essentially the same

results (**Figure S4**). In conclusion, loss of MCAD activity leads to an increase of medium-chain acyl-CoA esters, and a decrease in free CoA, short- and long-chain acyl-CoA, in agreement with the predicted sequestration of free CoA into medium-chain acyl-CoA esters.

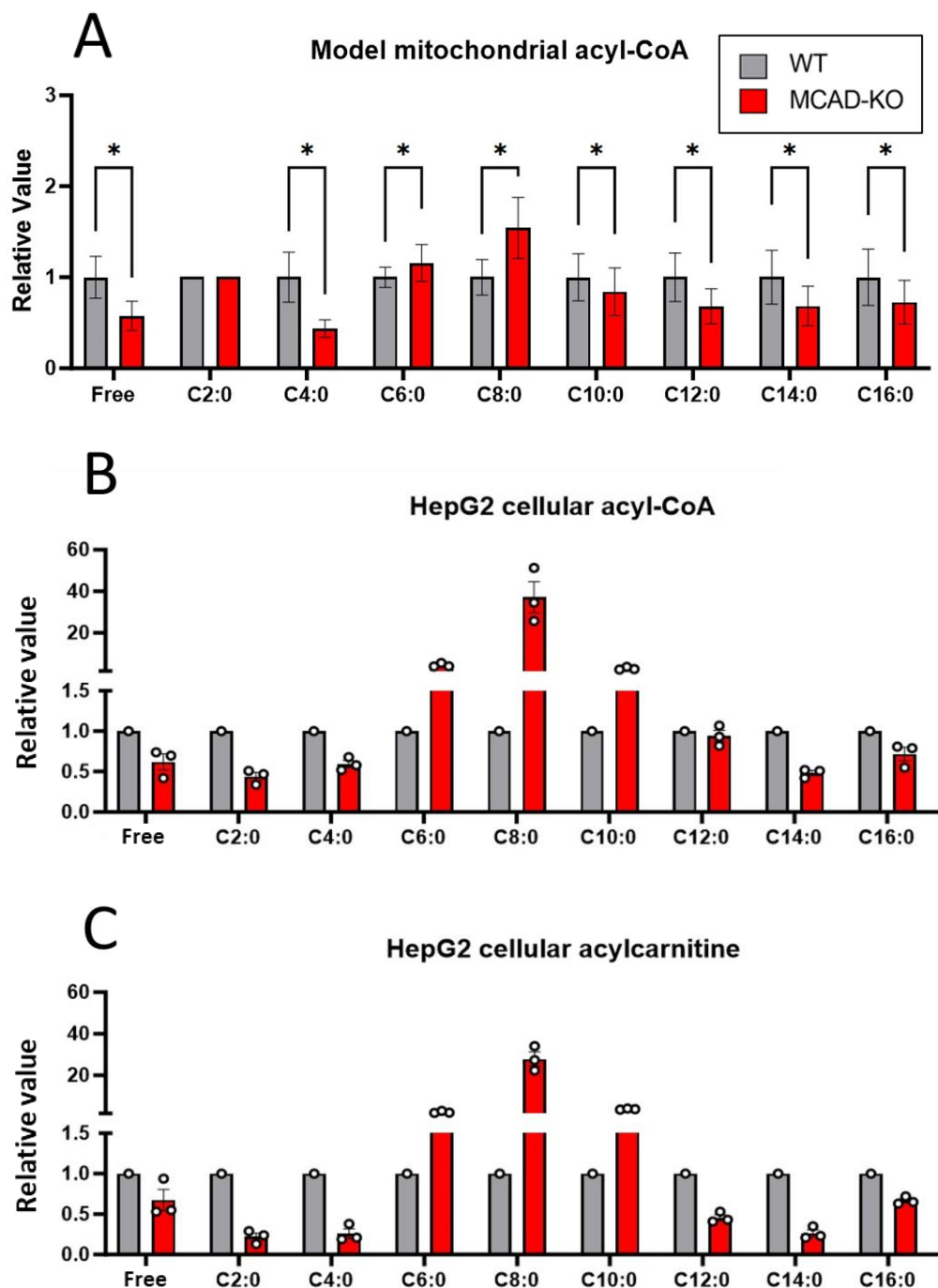


Figure 2. Acyl-CoA and acylcarnitine profile in computational model and HepG2 cells. **A.** Mitochondrial acyl-CoAs predicted by computational simulations of mFAO in human liver.* $p < 0.05$, matched-pair Wilcoxon tests.; **B.** Acyl-CoA esters in HepG2 cells.; **C.** Acylcarnitines in HepG2 cells. WT and MCAD-KO cells were cultured in *high-fat no-glucose medium* for 24 h (DMEM, 0 mM glucose, 0 mM pyruvate, 0 mM glutamine, supplemented with 0.5 mM palmitate and 2 mM L-carnitine). The grey bar represents WT cells while red bar represents MCAD-KO clone (each data point represent one KO clone-KO4, KO9, KO21). The data consists of mean of 3 independent experiments. In turn, each independent experiment consisted of 4-5 parallel cell cultures/technical replicates. (Error) bar represents median and range of the data. Expanded data sets are presented in **Figure S2 and S3**. The significance scores per experiment and per MCAD-KO clone for acyl-CoA and acylcarnitines in the HepG2 cells are detailed in the supplement (**Tables S4-S5**).

3.2 Loss of MCAD does not affect CoA biosynthesis

PANK, the first enzyme in the biosynthetic pathway of CoA, has been reported to be inhibited by acyl-CoA esters [2]. Therefore, we interrogated if CoA biosynthesis was affected by the knockout of MCAD in HepG2 cells. At time 0 h, mFAO substrates (palmitate and L-carnitine) were added and pantothenate, the precursor of CoA, was replaced by isotopically labelled $^{13}\text{C}_3^{15}\text{N}_1$ -pantothenate (**Figure 3A**). Confirming previous observations (**Figure 2B**), after 24 h incubation in the presence of palmitate and L-carnitine, MCAD-KO cells had lower levels of free CoA than their WT counterparts (**Figure 3B**). At time 0 h, without the addition of mFAO substrates, there was no difference between WT and MCAD-KO, demonstrating that the effect was depended on an active mFAO pathway (**Figure 3B**). The total CoA pool (acylated plus free fraction) did not differ between WT and MCAD-KO cells (**Figure 3C**). In line with this, there was no difference between the groups in the percentage of label incorporation over the course of 24 h, neither into the free fraction nor into the total CoA pool (**Figure 3D and 3E**). Remarkably, we detected approximately 10 times more label incorporation into the free CoA fraction than into the total CoA pool (**Figure 3D and 3E**), suggesting the existence of a large inert pool that is replaced at a much slower rate than the metabolically active pool. In conclusion, the fact that label incorporation and total CoA were not affected by the MCAD knockout, demonstrates that loss of MCAD did not affect the CoA biosynthesis rate in these HepG2 cells under the conditions studied.

Therefore, the reduced free CoA observed in MCAD-KO was not caused by a smaller total CoA pool, but the CoA sequestration into medium-chain acyl-CoA esters.

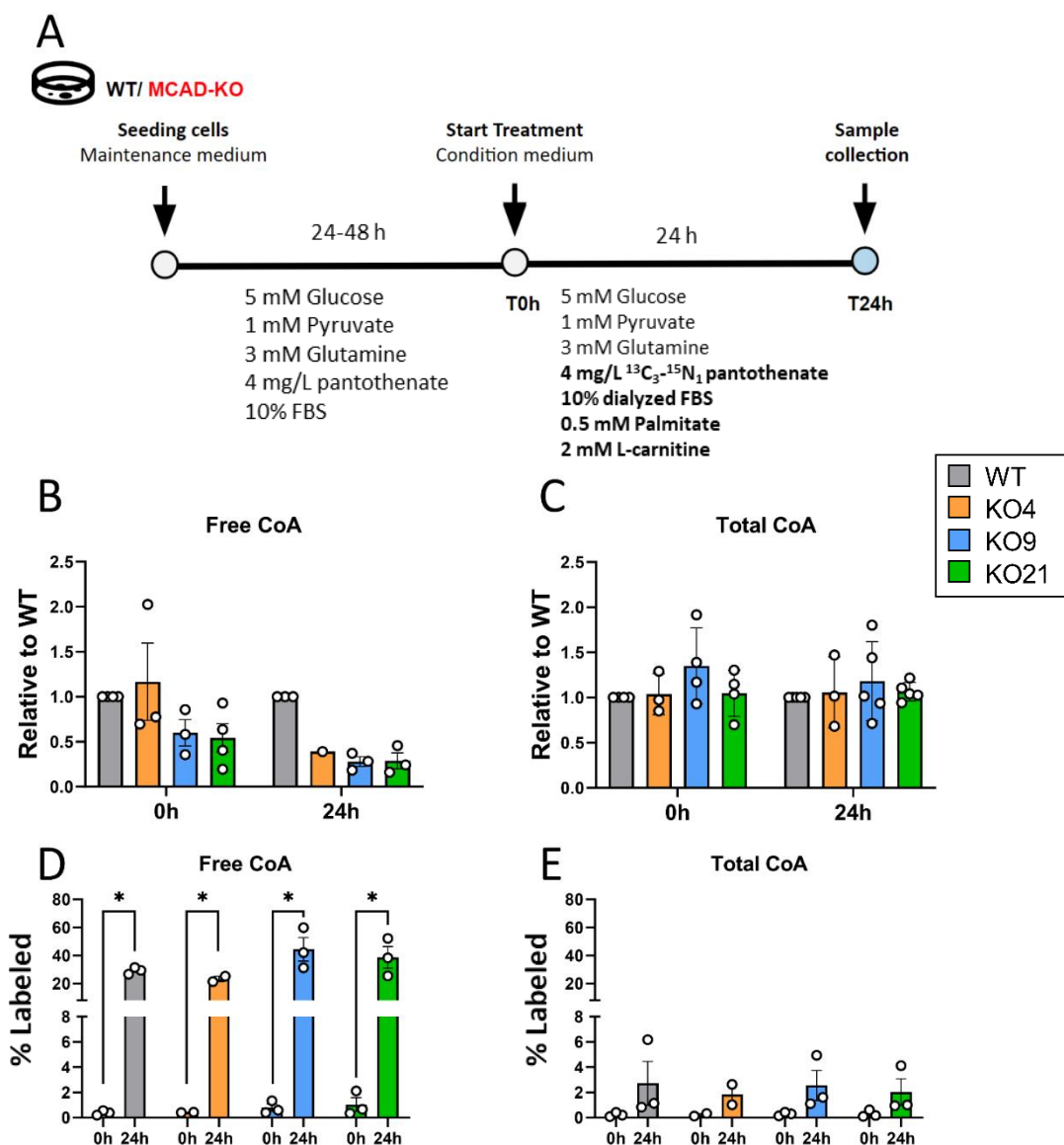


Figure 3. CoA biosynthesis in MCAD-KO cells. **A.** Simplified scheme of study design; After seeding, cells were precultured in maintenance medium (DMEM 5 mM glucose, 1 mM pyruvate, 3 mM glutamine, 4 mg/L pantothenate, 10% FBS). At T0h, the maintenance medium was replaced by a *high-fat low-glucose medium* (DMEM 5 mM glucose, 1 mM pyruvate, 3 mM glutamine, 10% dialyzed FBS, supplemented with 0.5 mM palmitate and 2.0 mM L-carnitine), in which non-labeled pantothenate was replaced by 4 mg/L stable isotope labeled pantothenate; After 24 h in condition medium, samples were collected at T24h.; **B & C.** Free and total CoA relative to WT.; **D & E.** Percentage label incorporation into the free and total CoA pools. * $p < 0.05$ with an unpaired t-test. For all experimental data (**B-E**), each datapoint represents an independent experiment, using a different cell passage (n=1-3). In turn, each individual experiment consisted of 4-5 technical replicates (parallel cell cultures). Therefore, each datapoint represents the average of 4-5 technical replicates, per experiment. For **B-C**, the values shown are relative to the average of the WT within the same experiment.

3.3 MCAD-KO mice remodel CoA metabolism under severe energetic stress

After validating the simulations *in vitro*, we set to investigate the effect of MCAD deficiency on the CoA pool and metabolism *in vivo*. Previous studies have reported that MCAD-KO mice, as MCADD patients, shows resistance when subjected only to fasting [43,44]. Recently, Martines ACMF et al. reported that the combination of fasting and cold exposure triggers relevant disease phenotype in MCAD-KO mice, such as reduced blood glucose, reduced amino acids and triglycerides accumulation in the liver [45]. In this context, we investigated hepatic CoA metabolism in young (8-weeks old) MCAD-KO mice upon fasting and cold exposure. Our experimental groups comprised WT and MCAD-KO littermate mice in all the three conditions: (1) fed, (2) 14 h overnight fasted, and (3) 14 h overnight fasted plus 4 h fasted at 4 °C (total of 18 h fasting) (**Figure 4A**). First, total CoA and CoA biosynthesis intermediate levels consisting of phosphopantetheine (P-Pant) and dephospho-CoA (dPCoA) were measured in liver samples (**Figure 4B and 4C**). Due to methodological limitations, we were not able to accurately measure free CoA and acyl-CoA profile in mice samples. In alignment with the literature [46], in both WT and MCAD-KO, P-Pant and total CoA levels were increased in response to fasting. Notably, a significant increase in total CoA levels was detected in MCAD-KO mice compared to WT mice after fasting and cold exposure. Taken together, the results suggest that CoA biosynthesis is affected by loss of MCAD, and specifically under energetic stress conditions.

To explore this further, the expression of genes involved in CoA metabolism were quantified. Indeed, mRNA levels encoding isoenzymes of the first enzyme in the CoA biosynthesis pathway (*Pank1a*, *Pank1b*, and *Pank3*) were upregulated in MCAD-KO relative to WT mice, when exposed to fasting plus cold (**Figure 4D**). The mRNA encoding *Pank4*, an enzyme that counteracts CoA biosynthesis by converting phosphopantetheine back to pantetheine [47], was significantly downregulated (**Figure 4D and S5A**). All these adaptations are therefore consistent with an effort to increase CoA levels. At the same time, the mRNA levels encoding the carnitine acyltransferases *Cpt1a*, *Cpt2*, and *Crat* were upregulated in MCAD-KO relative to WT mice (**Figure 4E**). These enzymes can release mitochondrial CoA by transferring acyl-groups to L-carnitine, forming acylcarnitines, which can cross the mitochondrial membrane (**Figure 1B**) [48,49]. The mRNA encoding the peroxisomal acyl-CoA transporter *Abcd1* was also upregulated. This might also decrease the burden on the mitochondrial CoA pool, allowing, instead, the peroxisome to take over some of the beta-oxidation that would normally take place in the mitochondria [32,50]. Upregulation of *Nudt19*, potentially involved in

detoxification of acyl-CoA esters (**Figure 1A**), was significant, but too small to be relevant (**Figure 4E**).

Finally, mRNA of several ACOT isoenzymes were substantially and significantly upregulated (**Figure 4F**), with even a 2- to 4-fold increase of *Acot2* and *Acot3* expression. Smaller, but still significant changes were seen for mRNAs encoding other isoenzymes with a median increase between 40% (*Acot8*) and 64% (*Acot 4* and *Acot7*). The same analyses were carried out in HepG2 cells under both *high-fat no-glucose* and *high-fat low-glucose medium* (**Figure S5 and S6, Table S6 and S7**), however, the changes were not consistent across the different MCAD-KO clones.

Altogether, the changes in gene expression observed in the liver of MCAD-KO mice exposed to fasting and cold seemed to work towards increasing the CoA synthesis and relieving the accumulation of acyl-CoA species.

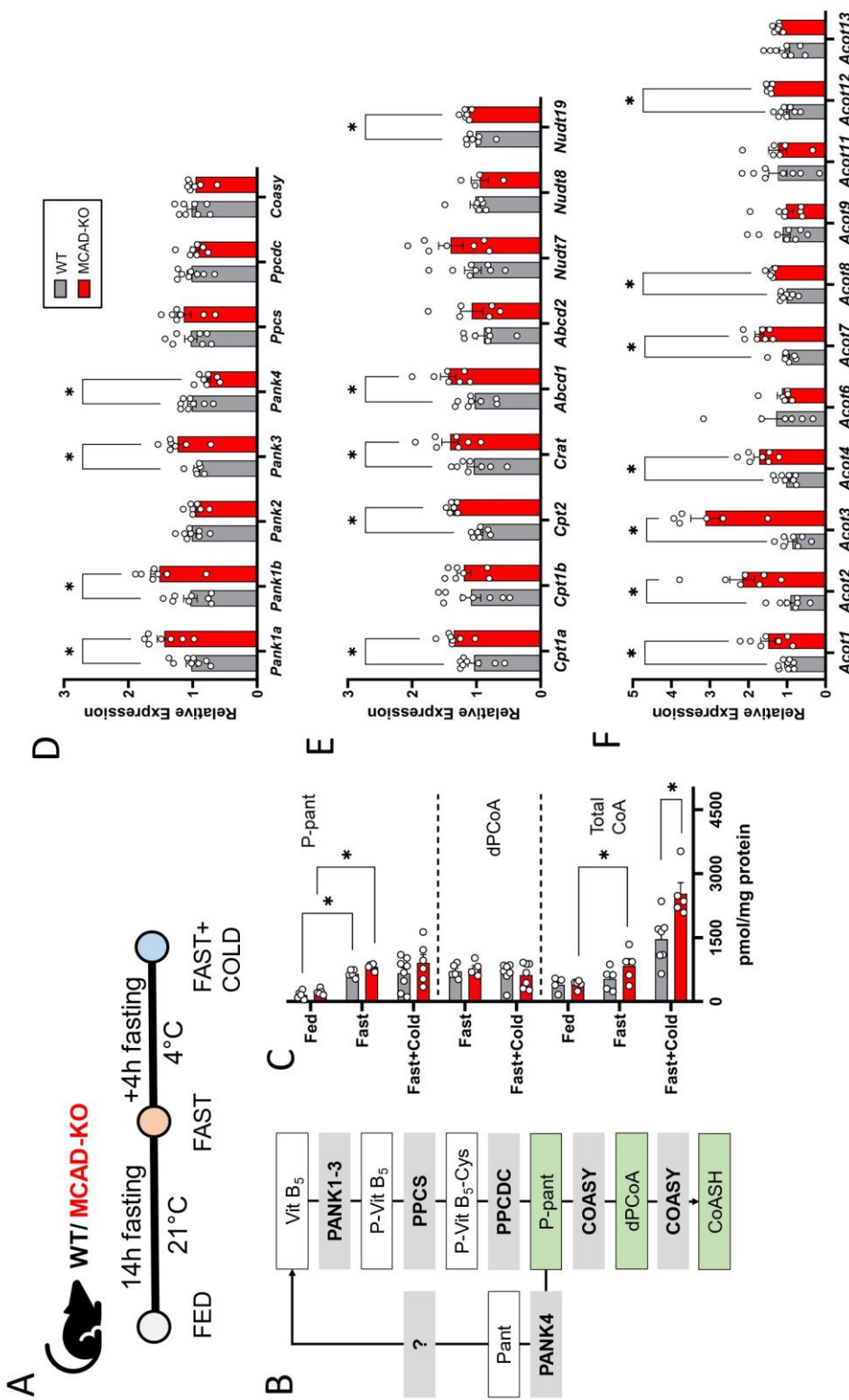


Figure 4. CoA metabolism in the liver of mice exposed to fasting and cold. **A.** Mice either had free access to food (fed), were fasted overnight for 14 h (fast), or fasted for 18 h of which the last 4 h at 4 °C (fast + cold); **B.** CoA biosynthesis pathway. PANK (gene *Pank*) = pantothenate kinase, PPCS (gene *Ppcs*) = phosphopantothenate-cysteine ligase, PPCDC (gene *Ppcdc*) = phosphopantothenoylcysteine decarboxylase, COASY (gene *Coasy*) = bifunctional coenzyme A synthase, Vit B₅ = pantothenate, P-Vit B₅-Cys = phosphopantothenoyl-cysteine, P-pant = phosphopantetheine, P-pant = phosphopantetheine, Pant = pantetheine, dPCoA = dephospho-CoA. Metabolites are shown in white or green boxes (green boxes correspond to data in panel C) and enzymes in grey.; **C.** Metabolites in the CoA biosynthesis pathway.; **D-F.** Hepatic gene expression in fasted, cold-exposed mice. mRNA levels relative to WT of CoA biosynthetic enzymes (**D**), acyltransferases and peroxisomal enzymes (**E**) and acyl-CoA thioesterases (**F**). * $p < 0.05$ using an unpaired t-test; ± standard error of the mean (SEM).

3.4 Combined upregulation of CoA biosynthesis and ACOT normalize CoA metabolites

Finally, we investigated how the increased total CoA levels in MCAD-KO relative to WT mice, and the upregulated *Acot* expression, affected the concentrations of free CoA and that of potentially toxic medium chain acyl-CoAs. The experimental analysis would only show the total cell average rather than the local mitochondrial concentration. Therefore, we turned again to the computational kinetic model of the mFAO. **Figure 5A** shows the simulated distribution of CoA over the acyl-CoA esters in WT and MCAD-KO in mitochondria. In agreement with **Figure 2**, C8-CoA sequestered most of the available CoA in the MCAD-KO, resulting in a reduced free CoA fraction. Interestingly, if the total CoA in the mutant was increased by 10%, from 3.60 mM to 3.96 mM (**Figure 5A**), the free CoA was restored to the WT level. Most of the extra CoA, however, ended up in the C8-CoA fraction, which was almost doubled.

Subsequently, we tested the effect of simultaneously increasing the total CoA concentration and the ACOT activity (**Figure 5B and 5C**). Again, at low ACOT activities, increasing total CoA almost doubled the levels C8-CoA in the MCAD-KO model (**Figure 5B**). Concomitantly, the free CoA fraction also increased, but to a smaller extent (**Figure 5C**). Increased ACOT activity reduced C8-CoA steeply, while at the same time increasing free CoA. The combined effect of elevated CoA and ACOT was more effective than either alone. However, a 20-fold increase of ACOT activity was required to completely normalize C8-CoA. Altogether, these results show that the observed upregulation of total CoA and ACOT are a powerful compensatory mechanism when MCAD activity is lost, yet not sufficient to fully normalize CoA metabolites.

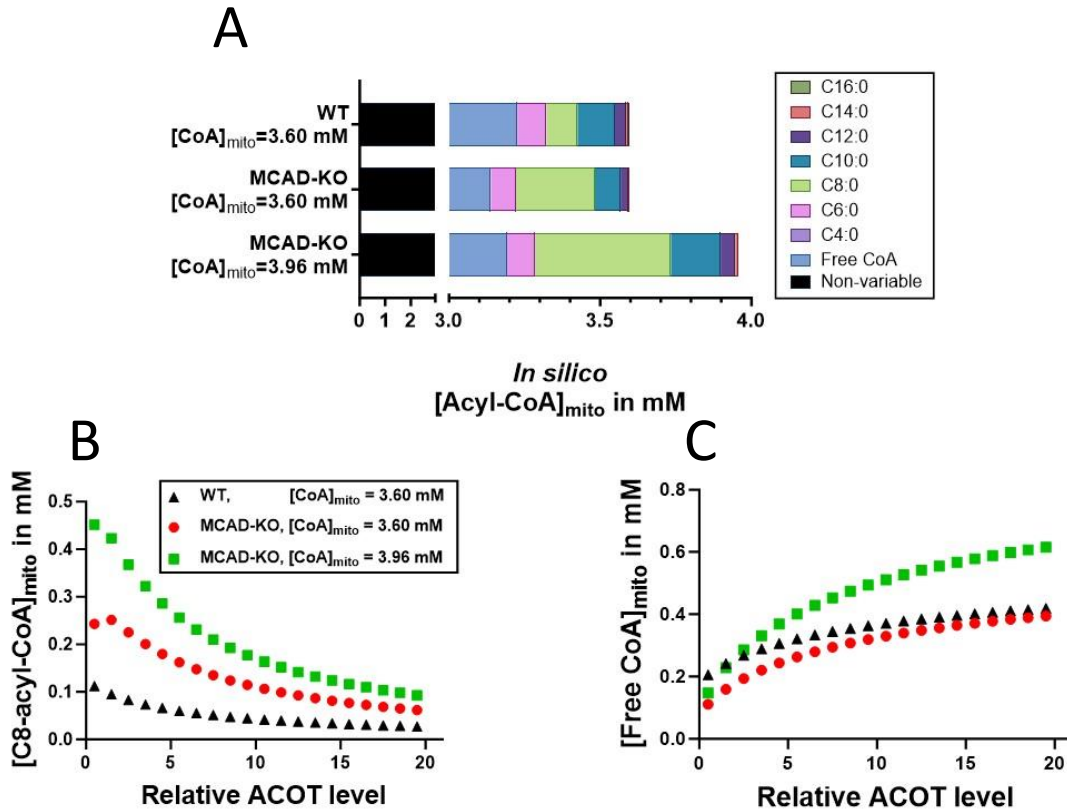


Figure 5. Increased total CoA and ACOT as compensation for free CoA depletion. *In silico* prediction of acyl-CoA and free CoA concentrations. Three models are compared: WT with 100% MCAD activity, MCAD-KO with 0% MCAD activity and MCAD-KO with elevated total CoA. **A.** Breakdown of the variable mitochondrial CoA pool. The non-variable pool represents a realistic amount of CoA that would be sequestered by mitochondrial pathways other than the mFAO.; **B & C.** Steady-state mitochondrial concentrations of C8-CoA (**B**) and free CoA (**C**), at increasing ACOT activity.

4. Discussion

Although depletion of the free CoA pool has been proposed as a pathogenic mechanism in MCADD, experimental evidence of this is largely absent [2–4,22]. The present study combined *in silico*, *in vitro* and *in vivo* approaches to further investigate it. Our *in silico* results suggested the sequestration of CoA as medium-chain acyl-CoA esters coincides with a decrease in free CoA. Additionally, the simulations have also shown that this phenotype could be remedied by increasing *de novo* production of CoA and by releasing existing CoA from acyl-CoAs. Our experimental results, both in cells and in animals, corroborated these computational predictions. The accumulation of medium-chain acyl-CoAs and concomitant indications of free CoA depletion in cells confirmed the validity of MCADD as a CASTOR disease. Gene expression data in both MCAD-KO cells and mice, as well as CoA measurements in fasted, cold-exposed MCAD-KO mice demonstrated a reorganisation of the CoA metabolism that

could be interpreted as an adaptation to increase the availability of free CoA and relieve the excessive accumulation of C8-CoA.

Computational modelling results suggested an accumulation of C8-CoA which takes up most of the mitochondrial CoA pool in MCAD-KO, leading to decreased levels of all other chain-lengths relative to the WT model including, the free CoA species (**Figure 2A**). The same pattern was seen in MCAD-KO HepG2 cells exposed in both *high-fat low-glucose* and *high-fat no-glucose medium* for 24 h (**Figure 2B and Figure S4A**). This evidence was in favour of the hypothesis that an extensive sequestration of CoA as medium-chain species in MCADD might underlie some of the symptomatology of MCADD patients in crisis [22]. Interestingly, both longer- and shorter-chain acyl-CoAs were decreased in MCAD-KO cells, as in the computational model. One might expect longer chains to also accumulate as they are upstream of the medium chains that constitute the bottleneck. However, the finding that long chains also decrease might suggest that a depletion of free CoA hampers the import of new long-chain substrates into the pathway. The implications of this for an MCADD patient might be dire: it would mean that most of the beta-oxidation substrates are in the least useful form, as medium chains, of which the oxidation is most impaired. This finding is a good example of how models assist us in generating and understanding counter-intuitive pathway behaviours [51].

Another relevant finding of this study was the confirmation that the acyl-CoA profile was mirrored in the acylcarnitines in these cells (**Figure 2C and Figure S4B**). This is important, as acylcarnitines, which cross the cell membrane to enter the bloodstream, are important clinical markers of MCADD and have always been assumed to mirror the cellular acyl-CoA profile [9,52]. Our results provide evidence of the appropriateness of acylcarnitines as proxies for acyl-CoAs.

An important note is that the computational model did not make any predictions with regard to acetyl-CoA, as this metabolite is a fixed parameter. However, acetyl-CoA is a crucial metabolite, and it is interesting to reflect on how a variable acetyl-CoA is expected to compare to *in vitro* measurements. In the cells, acetyl-CoA was about halved in the MCAD-KO cells relative to the WT. Acetyl-CoA from the mFAO is also crucial for the production of ketone bodies in the liver during periods of fasting [53,54]. A reduction in acetyl-CoA levels is therefore also a potential link between MCADD and hypoketosis. Future investigations should take the role of this metabolite into account.

Having obtained evidence for the initial hypothesis of free CoA depletion in MCAD-KO, we shifted our attention to adaptations in the broader network. One logical adaptation would be the upregulation of CoA synthesis. In our results, we obtained a decrease in free CoA for MCAD-KO cell lines compared to WT after palmitate and L-carnitine supplementation in *high-fat low-glucose medium* (**Figure 3B**). Conversely, we did not observe any difference in total CoA pools in these cells (**Figure 3C**). Previous studies on computational modelling suggested that the extensive sequestration of acyl-CoA esters and depletion of free CoA under fat overload conditions is a property of the mFAO even without the loss of MCAD, as it is a substrate of the pathway [10,24,55]. In our study, despite the same level of total CoA, the MCAD-KO cells exhibited a lower free CoA content than the WT cells in *high-fat low-glucose medium*. This might indicate that the production of new CoA was less effective at increasing the free CoA levels in KO cells than in WT cells, as part of the newly synthesized CoA might be channeled into C8-CoA in MCAD-KO cells. We observed higher label incorporation in free CoA as compared to total CoA pool. Additionally, we did not observe any difference in the label incorporation between WT and MCAD-KO groups (**Figure 3D and 3E**). Our observations suggest that the knockout of MCAD did not impact the rate of CoA biosynthesis or its total pool size in HepG2 cells under the examined conditions. If the total CoA pool was constantly used and recycled in the various CoA-consuming processes, then one would expect the fraction of labeled free and total CoA to be more or less equivalent. Instead, it seemed like there was a large portion of the total CoA pool which was not readily released as free CoA (which would reduce the fraction of labeled free CoA). The probable reasons might be that the CoAs are covalently attached to proteins (CoAlation [56]), or much of the cellular CoA is constituted of acyl-CoAs that are bound very tightly to high-affinity binding proteins that protect them from thioesterases and acyltransferases [57,58]. Further investigation is required to elucidate this question.

In vivo, the CoA level is dynamic, rapidly changing in response to the metabolic and feeding states. Under fasting condition, total CoA has been shown to increase in the liver [59], following a higher demand for this metabolite in active metabolic pathways such as fatty acid oxidation and gluconeogenesis. With regards to temperature, rats exposed to cold stress have been reported to present increased incorporation of labeled pantothenate and CoA synthesis in the liver [38]. Therefore, the combination of fasting and cold must impose a high demand for CoA on top of ATP requirements coming from thermogenesis [60]. Such condition might be particularly challenging in MCADD, which is predicted to have a lower mFAO flux and limited

CoA availability [10,22]. Indeed, despite their resistance to long-time fasting, MCAD KO mice have been shown to be cold-sensitive [43]. In our study, we observed a significant activation of CoA biosynthesis, carnitine acyltransferases and several ACOT enzymes that both release free CoA and alleviate excessive acyl-CoA accumulation highlighting both strategies and their relevance as compensatory mechanisms in MCADD. ACOTs are understood to have a regulatory function over the levels of acyl-CoAs, free fatty acids and free CoA in cells [61,62]. Most relevant for our hypothesis is the ACOTs ability to act as “a release valve when CoA is limiting” [27]. In HepG2 cells, MCAD-KO clone 9 (KO9) showed similar changes with those observed in the liver of MCAD KO-mice, suggesting an attempt to rescue the free CoA pool and alleviate excessive accumulation of C8-CoA. However, it should be noted that there was a considerable variation among the different MCAD-KO clones (**Figures S5 and S6, Table S6 and S7**). Unraveling the particularities of each MCAD-KO clone that led to its specific gene expression profile and investigating its precise impact on the acyl-CoA and free CoA levels were beyond the scope of this investigation.

The theme of our results has very much been one of simultaneous events having some shared underlying logic and mechanistic origin. The accumulation of medium-chain acyl-CoAs might have depleted the free CoA pool, which might trigger the production of more CoA. In the context of MCAD deficiency, however, the production of more CoA might simply lead to further accumulations in acyl-CoAs, possibly to toxic levels without much of a gain in free CoA [63]. Simultaneous processes for reducing the levels of acyl-CoA might therefore be engaged, for instance the upregulation of ACOTs. This hypothetical scenario was computationally modelled. However, one can imagine not two, but multiple mechanisms being simultaneously engaged to increase free CoA while avoiding the risk of lipotoxicity from an enlarged acyl-CoA pool. It is also possible, if not likely, that different MCAD-KO cell lines and animals, indeed different MCADD patients, might engage different sets of rescue mechanisms. This might be an important insight for understanding inter-patient heterogeneity better.

A significant limitation of the current study is that the models used differ in a number of important ways from an MCADD patient. Kinetic models by definition contain only a subset of the metabolic reactions and many potential adaptations and dangers might be excluded. In order to identify other possibilities, experimental models could be of great use. HepG2 cells, though useful and convenient to use, are only imperfect models of human liver cells. The development of 3D *in vitro* cultures, such as liver organoids [64–67] from induced pluripotent

stem cells might, in future, promise ways of generating more human liver-like *in vitro* cultures, especially if MCADD patient cells could be used. Another limitation is the broader physiological context: not only livers, but whole bodies are MCAD deficient, and this could have implications for the manifestation of the conditions. Animal models could help, but are also not perfect substitutes for human bodies. Patient studies like FiTtINg MCADD holds promise for yielding some human data collected under controlled conditions that might yield more insight [68].

5. Conclusion

In conclusion, we have described an approach in which *in silico*, *in vitro* and *in vivo* techniques were combined to confirm that loss of MCAD can indeed trigger a CASTOR phenotype. Our observations showed the sequestration of medium-chain acyl-CoA metabolites in MCAD-KO systems, potentially depletes free CoA during metabolic stress. We have also identified several rescue mechanisms that could mitigate this phenotype. Our gene expression analysis revealed the activation of CoA biosynthesis and acyl-CoA thioesterases as compensatory mechanisms that might increase free CoA levels, preventing excessive accumulation of acyl-CoA species. For future research, it is essential to consider the broader network in which MCADD and other CASTOR diseases operate. This broader network can respond, either in compensatory or in aggravating ways, to seemingly simple perturbations.

Author contributions

C.O., L.A.K., M.S., A.C.H., T.H., and B.M.B. designed the experiments. C.O., L.A.K., and M.S. performed the experiments, generated and interpreted the data, and wrote the manuscript. M.S. with the support of A.D., V.C. and G.L.F.K. developed, optimized and performed the HILIC-MS/MS protocol used in this work. C.O. performed all the computational simulations. M.L.M. supported with the *in vitro* experiments and qPCR analyses. M.v.d.Z. performed the HPLC analysis. A.C.M.F.M. and L.A.K. designed and conducted the animal experiments. N.C.A.H. and B.v.d.S. advised on the overexpression experiments, and N.C.A.H. and L.A.K. carried them out. A.G., H.S., D.J.R. and O.C.M.S provided important advice at various crucial junctures during experimental design and manuscript writing. A.C.H., T.H., and B.M.B. supervised the project and edited the draft manuscript. All authors commented on the text.

Declaration of competing interests

This paper has no conflict of interest with any of the other research groups, or organizations.

Acknowledgements

We would like to thank Maaïke H. Oosterveer, Matthias Ziegler and Eugenio Ferrario for many fruitful scientific discussions and advice. We would also like to acknowledge Victor Bernal and Venustiano Soancatl Aguilar, members of the Data Science Team from the University of Groningen, for the excellent support on the statistical analyses. This work was supported by the European Union's Horizon 2020 research and innovation program under the Marie Skłodowska-Curie grant agreement PoLiMeR, No. 812616.

References

- [1] J.L. Robinson, P. Kocabaş, H. Wang, P.-E. Cholley, D. Cook, A. Nilsson, M. Anton, R. Ferreira, I. Domenzain, V. Billa, A. Limeta, A. Hedin, J. Gustafsson, E.J. Kerkhoven, L.T. Svensson, B.O. Palsson, A. Mardinoglu, L. Hansson, M. Uhlén, J. Nielsen, An atlas of human metabolism, *Sci Signal*. 13 (2020) eaaz1482. <https://doi.org/10.1126/scisignal.aaz1482>.
- [2] G.A. Mitchell, N. Gauthier, A. Lesimple, S.P. Wang, O. Mamer, I. Qureshi, Hereditary and acquired diseases of acyl-coenzyme A metabolism, *Mol Genet Metab*. 94 (2008) 4–15. <https://doi.org/10.1016/j.ymgme.2007.12.005>.
- [3] H. Yang, C. Zhao, Y. Wang, S.P. Wang, G.A. Mitchell, Hereditary diseases of coenzyme A thioester metabolism, *Biochem Soc Trans*. 47 (2019) 149–155. <https://doi.org/10.1042/BST20180423>.
- [4] H. Yang, C. Zhao, M.-C. Tang, Y. Wang, S.P. Wang, P. Allard, A. Furtos, G.A. Mitchell, Inborn errors of mitochondrial acyl-coenzyme a metabolism: acyl-CoA biology meets the clinic, *Molecular Genetics and Metabolism*. 128 (2019) 30–44. <https://doi.org/10.1016/j.ymgme.2019.05.002>.
- [5] G.S. Ribas, F.F. Lopes, M. Deon, C.R. Vargas, Hyperammonemia in Inherited Metabolic Diseases, *Cell Mol Neurobiol*. 42 (2022) 2593–2610. <https://doi.org/10.1007/s10571-021-01156-6>.
- [6] E.A. Jager, M.M. Kuijpers, A.M. Bosch, M.F. Mulder, E.R. Gozalbo, G. Visser, M. de Vries, M. Williams, H.R. Waterham, F.J. van Spronsen, P.C.J.I. Schielen, T.G.J. Derks, A nationwide retrospective observational study of population newborn screening for medium-chain acyl-CoA dehydrogenase (MCAD) deficiency in the Netherlands, *J Inherit Metab Dis*. 42 (2019) 890–897. <https://doi.org/10.1002/jimd.12102>.
- [7] U. Spiekerkoetter, J. Vockley, Mitochondrial Fatty Acid Oxidation Disorders, in: N. Blau, C. Dionisi Vici, C.R. Ferreira, C. Vianey-Saban, C.D.M. van Karnebeek (Eds.), *Physician's Guide to the Diagnosis, Treatment, and Follow-Up of Inherited Metabolic Diseases*, Springer International Publishing, Cham, 2022: pp. 929–957. https://doi.org/10.1007/978-3-030-67727-5_48.
- [8] K. Tanaka, I. Yokota, P.M. Coates, A.W. Strauss, D.P. Kelly, Z. Zhang, N. Gregersen, B.S. Andresen, Y. Matsubara, D. Curtis, Mutations in the medium chain acyl-CoA dehydrogenase (MCAD) gene, *Hum Mutat*. 1 (1992) 271–279. <https://doi.org/10.1002/humu.1380010402>.
- [9] M.A. Nada, W.J. Rhead, H. Sprecher, H. Schulz, C.R. Roe, Evidence for Intermediate Channeling in Mitochondrial β -Oxidation (*), *Journal of Biological Chemistry*. 270 (1995) 530–535. <https://doi.org/10.1074/jbc.270.2.530>.
- [10] K. van Eunen, S.M.J. Simons, A. Gerding, A. Bleeker, G. den Besten, C.M.L. Touw, S.M. Houten, B.K. Groen, K. Krab, D.-J. Reijngoud, B.M. Bakker, Biochemical Competition Makes Fatty-Acid β -Oxidation Vulnerable to Substrate Overload, *PLoS Comput Biol*. 9 (2013) e1003186. <https://doi.org/10.1371/journal.pcbi.1003186>.
- [11] B. Wilcken, M. Haas, P. Joy, V. Wiley, M. Chaplin, C. Black, J. Fletcher, J. McGill, A. Boneh, Outcome of neonatal screening for medium-chain acyl-CoA dehydrogenase deficiency in Australia: a cohort study, *Lancet*. 369 (2007) 37–42. [https://doi.org/10.1016/S0140-6736\(07\)60029-4](https://doi.org/10.1016/S0140-6736(07)60029-4).
- [12] T.G.J. Derks, T.S. Boer, A. van Assen, T. Bos, J. Ruiters, H.R. Waterham, K.E. Niezen-Koning, R.J.A. Wanders, J.M.M. Rondeel, J.G. Loeber, L.P. Ten Kate, G.P.A. Smit, D.-J. Reijngoud, Neonatal screening for medium-chain acyl-CoA dehydrogenase (MCAD) deficiency in The Netherlands: the importance of enzyme analysis to ascertain true MCAD deficiency, *J Inherit Metab Dis*. 31 (2008) 88–96. <https://doi.org/10.1007/s10545-007-0492-3>.
- [13] M. Pourfarzam, A. Morris, M. Appleton, A. Craft, K. Bartlett, Neonatal screening for medium-chain acyl-CoA dehydrogenase deficiency, *Lancet*. 358 (2001) 1063–1064. [https://doi.org/10.1016/S0140-6736\(01\)06199-2](https://doi.org/10.1016/S0140-6736(01)06199-2).

- [14] M.L. Couce, D.E. Castiñeiras, J.D. Moure, J.A. Cocho, P. Sánchez-Pintos, J. García-Villoria, D. Quelhas, N. Gregersen, B.S. Andresen, A. Ribes, J.M. Fraga, Relevance of expanded neonatal screening of medium-chain acyl co-a dehydrogenase deficiency: outcome of a decade in galicia (Spain), *JIMD Rep.* 1 (2011) 131–136. https://doi.org/10.1007/8904_2011_28.
- [15] A.K. Iafolla, R.J. Thompson, C.R. Roe, Medium-chain acyl-coenzyme A dehydrogenase deficiency: clinical course in 120 affected children, *J Pediatr.* 124 (1994) 409–415. [https://doi.org/10.1016/s0022-3476\(94\)70363-9](https://doi.org/10.1016/s0022-3476(94)70363-9).
- [16] B. Wilcken, J. Hammond, M. Silink, Morbidity and mortality in medium chain acyl coenzyme A dehydrogenase deficiency., *Arch Dis Child.* 70 (1994) 410–412.
- [17] E.H. Touma, C. Charpentier, Medium chain acyl-CoA dehydrogenase deficiency., *Arch Dis Child.* 67 (1992) 142–145.
- [18] N. Gauthier, J.W. Wu, S.P. Wang, P. Allard, O.A. Mamer, L. Sweetman, A.B. Moser, L. Kratz, F. Alvarez, Y. Robitaille, F. Lépine, G.A. Mitchell, A Liver-Specific Defect of Acyl-CoA Degradation Produces Hyperammonemia, Hypoglycemia and a Distinct Hepatic Acyl-CoA Pattern, *PLOS ONE.* 8 (2013) e60581. <https://doi.org/10.1371/journal.pone.0060581>.
- [19] O.A. Shchelochkov, N. Carrillo, C. Venditti, Propionic Acidemia, in: M.P. Adam, J. Feldman, G.M. Mirzaa, R.A. Pagon, S.E. Wallace, L.J. Bean, K.W. Gripp, A. Amemiya (Eds.), *GeneReviews®*, University of Washington, Seattle, Seattle (WA), 1993. <http://www.ncbi.nlm.nih.gov/books/NBK92946/> (accessed November 16, 2023).
- [20] C. Subramanian, M.W. Frank, R. Tangallapally, M.-K. Yun, A. Edwards, S.W. White, R.E. Lee, C.O. Rock, S. Jackowski, Pantothenate kinase activation relieves coenzyme A sequestration and improves mitochondrial function in mice with propionic acidemia, *Sci Transl Med.* 13 (2021) eabf5965. <https://doi.org/10.1126/scitranslmed.abf5965>.
- [21] C. Subramanian, M.W. Frank, R. Tangallapally, M.-K. Yun, S.W. White, R.E. Lee, C.O. Rock, S. Jackowski, Relief of CoA sequestration and restoration of mitochondrial function in a mouse model of propionic acidemia, *J Inherit Metab Dis.* 46 (2023) 28–42. <https://doi.org/10.1002/jimd.12570>.
- [22] K. van Eunen, C.M.L. Volker-Touw, A. Gerding, A. Bleeker, J.C. Wolters, W.J. van Rijt, A.-C.M.F. Martines, K.E. Niezen-Koning, R.M. Heiner, H. Permentier, A.K. Groen, D.-J. Reijngoud, T.G.J. Derks, B.M. Bakker, Living on the edge: substrate competition explains loss of robustness in mitochondrial fatty-acid oxidation disorders, *BMC Biol.* 14 (2016) 1–15. <https://doi.org/10.1186/s12915-016-0327-5>.
- [23] C. Odendaal, E.A. Jager, A.-C.M.F. Martines, M.A. Vieira-Lara, N.C.A. Huijman, L.A. Kiyuna, A. Gerding, J.C. Wolters, R. Heiner-Fokkema, K. van Eunen, T.G.J. Derks, B.M. Bakker, Personalised modelling of clinical heterogeneity between medium-chain acyl-CoA dehydrogenase patients, *BMC Biol.* 21 (2023) 1–22. <https://doi.org/10.1186/s12915-023-01652-9>.
- [24] A.-C.M.F. Martines, K. van Eunen, D.-J. Reijngoud, B.M. Bakker, The promiscuous enzyme medium-chain 3-keto-acyl-CoA thiolase triggers a vicious cycle in fatty-acid beta-oxidation, *PLoS Comput Biol.* 13 (2017) e1005461. <https://doi.org/10.1371/journal.pcbi.1005461>.
- [25] M. Singh, H.L. Elfrink, A.C. Harms, T. Hankemeier, Recent developments in the analytical approaches of acyl-CoAs to assess their role in mitochondrial fatty acid oxidation disorders, *Molecular Genetics and Metabolism.* (2023) 107711. <https://doi.org/10.1016/j.ymgme.2023.107711>.
- [26] M. Singh, L.A. Kiyuna, C. Odendaal, B.M. Bakker, A.C. Harms, T. Hankemeier, Development of targeted hydrophilic interaction liquid chromatography-tandem mass spectrometry method for acyl-Coenzyme A covering short- to long-chain species in a single analytical run, *Journal of Chromatography A.* (2023) 464524. <https://doi.org/10.1016/j.chroma.2023.464524>.
- [27] C. Bekeova, L. Anderson-Pullinger, K. Boye, F. Boos, Y. Sharpadskaya, J.M. Herrmann, E.L. Seifert, Multiple mitochondrial thioesterases have distinct tissue and substrate specificity and CoA regulation, suggesting unique functional roles, *J Biol Chem.* 294 (2019) 19034–19047. <https://doi.org/10.1074/jbc.RA119.010901>.
- [28] J.D. McGarry, C. Robles-Valdes, D.W. Foster, Role of carnitine in hepatic ketogenesis., *Proc Natl Acad Sci U S A.* 72 (1975) 4385–4388.
- [29] Y.-M. Zhang, S. Chohnan, K.G. Virga, R.D. Stevens, O.R. Ilkayeva, B.R. Wenner, J.R. Bain, C.B. Newgard, R.E. Lee, C.O. Rock, S. Jackowski, Chemical knockout of pantothenate kinase reveals the metabolic and genetic program responsible for hepatic coenzyme A homeostasis, *Chem Biol.* 14 (2007) 291–302. <https://doi.org/10.1016/j.chembiol.2007.01.013>.
- [30] R.R. Ramsay, R.D. Gandour, F.R. van der Leij, Molecular enzymology of carnitine transfer and transport, *Biochimica et Biophysica Acta (BBA) - Protein Structure and Molecular Enzymology.* 1546 (2001) 21–43. [https://doi.org/10.1016/S0167-4838\(01\)00147-9](https://doi.org/10.1016/S0167-4838(01)00147-9).
- [31] R. Leonardi, Y.-M. Zhang, C.O. Rock, S. Jackowski, Coenzyme A: back in action, *Prog Lipid Res.* 44 (2005) 125–153. <https://doi.org/10.1016/j.plipres.2005.04.001>.

- [32] M. Schrader, J. Costello, L.F. Godinho, M. Islinger, Peroxisome-mitochondria interplay and disease, *J Inherit Metab Dis.* 38 (2015) 681–702. <https://doi.org/10.1007/s10545-015-9819-7>.
- [33] G. Agrimi, A. Russo, P. Scarcia, F. Palmieri, The human gene SLC25A17 encodes a peroxisomal transporter of coenzyme A, FAD and NAD⁺, *Biochem J.* 443 (2012) 241–247. <https://doi.org/10.1042/BJ20111420>.
- [34] F. Palmieri, M. Monné, G. Fiermonte, L. Palmieri, Mitochondrial transport and metabolism of the vitamin B-derived cofactors thiamine pyrophosphate, coenzyme A, FAD and NAD⁺, and related diseases: A review, *IUBMB Life.* 74 (2022) 592–617. <https://doi.org/10.1002/iub.2612>.
- [35] G. Fiermonte, E. Paradies, S. Todisco, C.M.T. Marobbio, F. Palmieri, A Novel Member of Solute Carrier Family 25 (SLC25A42) Is a Transporter of Coenzyme A and Adenosine 3',5'-Diphosphate in Human Mitochondria, *J Biol Chem.* 284 (2009) 18152–18159. <https://doi.org/10.1074/jbc.M109.014118>.
- [36] S.D. Vickers, S.A. Shumar, D.C. Saporito, A. Kunovac, Q.A. Hathaway, B. Mintmier, J.A. King, R.D. King, V.M. Rajendran, A.M. Infante, J.M. Hollander, R. Leonardi, NUDT7 regulates total hepatic CoA levels and the composition of the intestinal bile acid pool in male mice fed a Western diet, *J Biol Chem.* 299 (2023) 102745. <https://doi.org/10.1016/j.jbc.2022.102745>.
- [37] S.A. Shumar, E.W. Kerr, P. Fagone, A.M. Infante, R. Leonardi, Overexpression of Nudt7 decreases bile acid levels and peroxisomal fatty acid oxidation in the liver, *J Lipid Res.* 60 (2019) 1005–1019. <https://doi.org/10.1194/jlr.M092676>.
- [38] M. Tsujikawa, S. Kimura, Effect of exposure to cold on pantothenic acid metabolism in rat liver, *Tohoku J Exp Med.* 133 (1981) 457–460. <https://doi.org/10.1620/tjem.133.457>.
- [39] M. Peters, J.J. Eicher, D.D. van Niekerk, D. Waltemath, J.L. Snoep, The JWS online simulation database, *Bioinformatics.* 33 (2017) 1589–1590. <https://doi.org/10.1093/bioinformatics/btw831>.
- [40] JWS Online: odendaal1. Available from: <https://www.jjj.bio.vu.nl/models/odendaal1/simulate/>, (n.d.).
- [41] B. Srinivasan, M. Baratashvili, M. Van Der Zwaag, B. Kanon, C. Colombelli, R.A. Lambrechts, O. Schaap, E.A. Nollen, A. Podgoršek, G. Kosec, H. Petković, S. Hayflick, V. Tiranti, D.-J. Reijngoud, N.A. Grzeschik, O.C.M. Sibon, Extracellular 4'-phosphopantetheine is a source for intracellular coenzyme A synthesis, *Nat Chem Biol.* 11 (2015) 784–792. <https://doi.org/10.1038/nchembio.1906>.
- [42] H. Wu, A.D. Southam, A. Hines, M.R. Viant, High-throughput tissue extraction protocol for NMR- and MS-based metabolomics, *Anal Biochem.* 372 (2008) 204–212. <https://doi.org/10.1016/j.ab.2007.10.002>.
- [43] R.J. Tolwani, D.A. Hamm, L. Tian, J.D. Sharer, J. Vockley, P. Rinaldo, D. Matern, T.R. Schoeb, P.A. Wood, Medium-Chain Acyl-CoA Dehydrogenase Deficiency in Gene-Targeted Mice, *PLoS Genet.* 1 (2005) e23. <https://doi.org/10.1371/journal.pgen.0010023>.
- [44] H. Herrema, T.G.J. Derks, T.H. van Dijk, V.W. Bloks, A. Gerding, R. Havinga, U.J.F. Tietge, M. Müller, G.P.A. Smit, F. Kuipers, D.-J. Reijngoud, Disturbed hepatic carbohydrate management during high metabolic demand in medium-chain acyl-CoA dehydrogenase (MCAD)-deficient mice, *Hepatology.* 47 (2008) 1894–1904. <https://doi.org/10.1002/hep.22284>.
- [45] Martines A-C. Exploring the mechanisms underlying the phenotype of MCAD deficiency with Systems Medicine: from computational model to mice to man. [Groningen]: Rijksuniversiteit Groningen, 2019. 275 p., (n.d.).
- [46] R. Leonardi, J.E. Rehg, C.O. Rock, S. Jackowski, Pantothenate Kinase 1 Is Required to Support the Metabolic Transition from the Fed to the Fasted State, *PLOS ONE.* 5 (2010) e11107. <https://doi.org/10.1371/journal.pone.0011107>.
- [47] C.C. Dibble, S.A. Barritt, G.E. Perry, E.C. Lien, R.C. Geck, S.E. DuBois-Coyne, D. Bartee, T.T. Zengeya, E.B. Cohen, M. Yuan, B.D. Hopkins, J.L. Meier, J.G. Clohessy, J.M. Asara, L.C. Cantley, A. Toker, PI3K drives the de novo synthesis of coenzyme A from vitamin B5, *Nature.* 608 (2022) 192–198. <https://doi.org/10.1038/s41586-022-04984-8>.
- [48] S. Violante, L. Ijlst, H. Te Brinke, I. Tavares de Almeida, R.J.A. Wanders, F.V. Ventura, S.M. Houten, Carnitine palmitoyltransferase 2 and carnitine/acylcarnitine translocase are involved in the mitochondrial synthesis and export of acylcarnitines, *FASEB J.* 27 (2013) 2039–2044. <https://doi.org/10.1096/fj.12-216689>.
- [49] C. Indiveri, V. Iacobazzi, A. Tonazzi, N. Giangregorio, V. Infantino, P. Convertini, L. Console, F. Palmieri, The mitochondrial carnitine/acylcarnitine carrier: function, structure and physiopathology, *Mol Aspects Med.* 32 (2011) 223–233. <https://doi.org/10.1016/j.mam.2011.10.008>.
- [50] M. Fransen, C. Lismont, P. Walton, The Peroxisome-Mitochondria Connection: How and Why?, *Int J Mol Sci.* 18 (2017) 1126. <https://doi.org/10.3390/ijms18061126>.
- [51] P.A. Saa, L.K. Nielsen, Formulation, construction and analysis of kinetic models of metabolism: A review of modelling frameworks, *Biotechnology Advances.* 35 (2017) 981–1003. <https://doi.org/10.1016/j.biotechadv.2017.09.005>.
- [52] E.P. Brass, C.L. Hoppel, Relationship between acid-soluble carnitine and coenzyme A pools in vivo, *Biochem J.* 190 (1980) 495–504.

- [53] J.A. Fletcher, S. Deja, S. Satapati, X. Fu, S.C. Burgess, J.D. Browning, Impaired ketogenesis and increased acetyl-CoA oxidation promote hyperglycemia in human fatty liver, *JCI Insight*. 4 (n.d.) e127737. <https://doi.org/10.1172/jci.insight.127737>.
- [54] C. Des Rosiers, F. David, M. Garneau, H. Brunengraber, Nonhomogeneous labeling of liver mitochondrial acetyl-CoA, *Journal of Biological Chemistry*. 266 (1991) 1574–1578. [https://doi.org/10.1016/S0021-9258\(18\)52332-2](https://doi.org/10.1016/S0021-9258(18)52332-2).
- [55] F. Abegaz, A.-C.M.F. Martines, M.A. Vieira-Lara, M. Rios-Morales, D.-J. Reijngoud, E.C. Wit, B.M. Bakker, Bistability in fatty-acid oxidation resulting from substrate inhibition, *PLoS Comput Biol*. 17 (2021) e1009259. <https://doi.org/10.1371/journal.pcbi.1009259>.
- [56] I. Gout, Coenzyme A, protein CoAlation and redox regulation in mammalian cells, *Biochem Soc Trans*. 46 (2018) 721–728. <https://doi.org/10.1042/BST20170506>.
- [57] C.A. Jolly, D.C. Wilton, F. Schroeder, Microsomal fatty acyl-CoA transacylation and hydrolysis: fatty acyl-CoA species dependent modulation by liver fatty acyl-CoA binding proteins, *Biochim Biophys Acta*. 1483 (2000) 185–197. [https://doi.org/10.1016/s1388-1981\(99\)00170-5](https://doi.org/10.1016/s1388-1981(99)00170-5).
- [58] J.T. Rasmussen, N.J. Faergeman, K. Kristiansen, J. Knudsen, Acyl-CoA-binding protein (ACBP) can mediate intermembrane acyl-CoA transport and donate acyl-CoA for beta-oxidation and glycerolipid synthesis, *Biochem J*. 299 (Pt 1) (1994) 165–170. <https://doi.org/10.1042/bj2990165>.
- [59] P. Naquet, E.W. Kerr, S.D. Vickers, R. Leonardi, Regulation of coenzyme A levels by degradation: the ‘Ins and Outs,’ *Prog Lipid Res*. 78 (2020) 101028. <https://doi.org/10.1016/j.plipres.2020.101028>.
- [60] F. Haman, F. Péronnet, G.P. Kenny, D. Massicotte, C. Lavoie, C. Scott, J.-M. Weber, Effect of cold exposure on fuel utilization in humans: plasma glucose, muscle glycogen, and lipids, *Journal of Applied Physiology*. 93 (2002) 77–84. <https://doi.org/10.1152/jappphysiol.00773.2001>.
- [61] B. Kirkby, N. Roman, B. Kobe, S. Kellie, J.K. Forwood, Functional and structural properties of mammalian acyl-coenzyme A thioesterases, *Prog Lipid Res*. 49 (2010) 366–377. <https://doi.org/10.1016/j.plipres.2010.04.001>.
- [62] M.C. Hunt, S.E.H. Alexson, The role Acyl-CoA thioesterases play in mediating intracellular lipid metabolism, *Prog Lipid Res*. 41 (2002) 99–130. [https://doi.org/10.1016/s0163-7827\(01\)00017-0](https://doi.org/10.1016/s0163-7827(01)00017-0).
- [63] Roe CR, Roe CR, Ding J. Mitochondrial fatty acid oxidation disorders. In: Scriver CR, Beaudet AL, Sly WS, Valle D, Childs B, Kinzler KW, et al., editors. *The Metabolic and Molecular Bases of Inherited Disease*. 8th ed. New York, NY: McGraw-Hill; 2001. p. 2297–326., in: *The Metabolic and Molecular Bases of Inherited Disease*., 8th ed., McGraw-Hill, n.d.: pp. 2297–326.
- [64] F. Sampaziotis, M.C. de Brito, P. Madrigal, A. Bertero, K. Saeb-Parsy, F.A.C. Soares, E. Schrupf, E. Melum, T.H. Karlsen, J.A. Bradley, W.T. Gelson, S. Davies, A. Baker, A. Kaser, G.J. Alexander, N.R.F. Hannan, L. Vallier, Cholangiocytes derived from human induced pluripotent stem cells for disease modeling and drug validation, *Nat Biotechnol*. 33 (2015) 845–852. <https://doi.org/10.1038/nbt.3275>.
- [65] Y. Guan, D. Xu, P.M. Garfin, U. Ehmer, M. Hurwitz, G. Enns, S. Michie, M. Wu, M. Zheng, T. Nishimura, J. Sage, G. Peltz, Human hepatic organoids for the analysis of human genetic diseases, *JCI Insight*. 2 (2017) e94954, 94954. <https://doi.org/10.1172/jci.insight.94954>.
- [66] S. Wang, X. Wang, Z. Tan, Y. Su, J. Liu, M. Chang, F. Yan, J. Chen, T. Chen, C. Li, J. Hu, Y. Wang, Human ESC-derived expandable hepatic organoids enable therapeutic liver repopulation and pathophysiological modeling of alcoholic liver injury, *Cell Res*. 29 (2019) 1009–1026. <https://doi.org/10.1038/s41422-019-0242-8>.
- [67] F. Wu, D. Wu, Y. Ren, Y. Huang, B. Feng, N. Zhao, T. Zhang, X. Chen, S. Chen, A. Xu, Generation of hepatobiliary organoids from human induced pluripotent stem cells, *J Hepatol*. 70 (2019) 1145–1158. <https://doi.org/10.1016/j.jhep.2018.12.028>.
- [68] T.G.J. Derks, Fasting Tolerance in Patients With Medium-chain Acyl-CoA Dehydrogenase Deficiency (MCADD) in the First Six Months of Life: an Investigator-initiated Human Pilot-study, clinicaltrials.gov, 2019. <https://clinicaltrials.gov/study/NCT03761693> (accessed January 1, 2023).

Supplementary material

MCAD overexpression in MCAD-KO HepG2 cells

HepG2 cells overexpressing *ACADM* were generated using the Polyethylenimine (PEI) transfection system and lentivirus. HEK293 cells were used as a lentivirus-producer cell line. Briefly, HEK293 cells were cultured in DMEM, supplemented with Glutamax I (Gibco, 31966-047), 10% FBS (Hyclone, SV30160) and 1% Penicillin-Streptomycin (10000 U/mL; Gibco, 15140122), and kept at 37 °C, 5% CO₂. For transfection, HEK293 cells were seeded into a 6-well plate at ~70% confluence. HEK293 cells were co-transfected with a mix of plasmids containing genes encoding lentivirus envelope (pHCMV-G, encoding for VSV-G behind a H-CMV promoter; ATCC, 75497), packaging (pMDLg/pRRE, include Gag and Pol genes; Addgene, 12251; pRSV-Rev, includes Rev gene; Addgene, 12253), and pGenLenti containing the target human *ACADM* gene (Genscript, U4143IC010) or control vector. Empty transfer vector (pCDH-CMV-MCS-EF1, System Biosciences, CD510B-1) was used as a negative control. EGFP-expressing plasmid (pLenti 9) was used as a positive control for transfection and transduction. The DNA-PEI mix contained: 440 µL DMEM (Glutamax I, 1% Penicillin-Streptomycin, no FBS), 60 µL PEI (1 mg/ml, pH 7.9, linear MW-25,000; Polysciences, 23966-2), and 3 µg of each plasmid. HEK293 cells were incubated with the mix for 24 h, and the supernatant was collected, filtered and supplemented with 5 µL Polybrene (8 mg/ml in H₂O; Sigma, H9268-5G). The filtered medium-containing virus was added to the target HepG2 cells, which were incubated for 24 h at 37 °C, 5% CO₂. This step was repeated 2 times. In total, HepG2 cells were incubated with a medium-containing virus for 48 h. Then this medium was replaced for DMEM medium (10% FBS, Glutamax I, 1% Penicillin-Streptomycin). Lastly, transduced HepG2 cells were selected using Puromycin for approximately 5-7 days (1.5 µg/ml).

Protein extraction and Immunoblotting

Cells were lysed in RIPA buffer (1% IGEPAL CA-630, 0.1% SDS, and 0.5% sodium deoxycholate in PBS) supplemented with Phosphatase Inhibitor Cocktail 2 (Sigma, P5726) and Cocktail 3 (Sigma, P0044) and Complete Protease Inhibitor Cocktail (Sigma, 1186145001). Lysate was sonicated using Sonics Vibra cell VCX130 (Sonics & Materials Inc.) (30 sec; pulses 1 sec on, 1 sec off; 40% amplitude), then centrifuged at 12000 rcf for 10 min at 4 °C. Protein content was determined using Pierce BCA Protein Assay Kit (ThermoScientific, 23225). Lysates were adjusted with Laemmli loading buffer (5X: 60 mM Tris-Cl pH 6.8, 10% glycerol, 1% SDS, 0.05% Bromophenol Blue, 1% beta-mercaptoethanol). Protein separation was done in SDS-PAGE 10% using a Mini PROTEAN Tetra Vertical Electrophoresis Cell system (Bio-Rad, 1658029FC). For immunoblotting, the following primary antibodies were used: MCAD (Abcam, AB92461) and HSP90.

Acyl-CoA and acylcarnitine extraction from HepG2 cells

HepG2 cells were subjected to a two-step extraction process using chloroform/methanol/water. HepG2 cells were provided with 100 µL of methanol. Prior to extraction, a mixture of 10 µL of acyl-CoA and acylcarnitine internal standards (Acetyl-1,2-¹³C₂-CoA, C7:0 CoA, C15:0 CoA, C17:0 CoA, L-carnitine-d₃, propionyl-L-carnitine-d₃, butyryl-L-carnitine-d₃, octanoyl-L-carnitine-d₃ and octadecanoyl-L-carnitine-d₃) was added to the study samples and vortexed for 1 min. Subsequently, 220 µL of methanol and 100 µL of water were added to each sample, followed by vortexing for 2 min and sonication for 3 min. To each sample, 320 µL of chloroform and 188 µL of water were added, vortexed for 2 min, and allowed to partition on ice for 10 min. The samples were then

centrifuged for 15 min at 4 °C with a speed of 15800 rcf. The resulting upper aqueous layer (450 µL) was transferred to a new Eppendorf tube. Additionally, the lower organic layer (250 µL) was transferred to the same Eppendorf tube. The combined solution was completely evaporated using a Labconco CentriVap vacuum concentrator (Kansas City, MO, USA). Following evaporation, the samples were reconstituted in a mixture of methanol/water/isopropanol (1:1:1, v/v/v) to a final volume of 100 µL, vortexed and centrifuged for 10 min. The supernatant was transferred to the HPLC vial for LC-MS injection.

Settings and configuration of HILIC-MS/MS method for analyzing free CoA and acyl-CoAs

For the acyl-CoAs, the separation of compounds was achieved using a mobile phase system consisting of acetonitrile:water (9:1) and 5 mM ammonium acetate for mobile phase A (MP-A), and acetonitrile:water (1:9) and 5 mM ammonium acetate for mobile phase B (MP-B). The flow rate was set at 0.25 mL/min, the autosampler temperature was maintained at 10 °C, and the column temperature was set to 40 °C. A 5 µL injection volume was used. The gradient elution method, spanning a 20 min duration, is provided in **Table S1.1**.

Table S1.1. Gradient program for acyl-CoA profiling

Time (min)	0	2.3	8.5	13.0	15.5	15.6	20.0
MP-A (%)	95.0	95.0	25.0	15.0	15.0	95.0	95.0
MP-B (%)	5.0	5.0	75.0	85.0	85.0	5.0	5.0

The QTRAP 6500 mass spectrometer was used in positive electrospray ionization mode. The mass spectrometer was configured with the following settings: the curtain gas (N₂) pressure was set to 25 psi, and the collision gas (N₂) was maintained at a medium level. The ion spray voltage was set at 4000 V. The source temperature was maintained at 325 °C, while the GS1 and GS2 pressures were set 60 psi. Data acquisition for targeted analysis was performed using scheduled MRM (sMRM) with a target scan time of 0.35 sec.

Settings and configuration of RPLC-MS/MS method for analyzing acylcarnitines

For the separation of acylcarnitines by RPLC, the mobile phase A (MP-A) consisted of 0.1% formic acid in water, while mobile phase B (MPB) contained 0.1% formic acid in acetonitrile. The injection volume was set at 5 µL, and the autosampler temperature was maintained at 10 °C, while the column temperature was set to 60 °C. A flow rate of 0.7 mL/min was employed. The gradient elution profile is provided in **Table S1.2**.

Table S1.2. Gradient program for acylcarnitine profiling

Time (min)	0	1.10	1.11	2.00	8.00	8.01	9.01	9.20	11.00
MP-A (%)	95.0	95.0	89.0	89.0	30.0	0	0	95.0	95.0
MP-B (%)	5.0	5.0	11.0	11.0	70.0	100.0	100.0	5.0	5.0

The QTRAP 6500 mass spectrometer was operated with the following parameters: the curtain gas (N₂) pressure was set to 20 psi, and the collision gas (N₂) was maintained at a medium level. For positive ion mode, the ion spray voltage was set at 4500 V. The source temperature was maintained at 350 °C, while the GS1 and GS2 pressures were set to 80 and 70 psi, respectively. Data acquisition for targeted analysis was performed using scheduled MRM (sMRM) with a target scan time of 0.1 sec.

The peak integration for both acyl-CoA and acylcarnitines was performed using AB Sciex OS (version 2.1.6, AB SCIEX, Concord, ON, Canada).

Total CoA measurements in mice samples

500 μL MilliQ H_2O was added to 25-100 mg liver tissue (adjusted to a final concentration of 0.2 mg liver/ μL), and the tissue was lysed using a tissue homogenizer (Precellys, Bertin Instruments) (6000 rpm, 15 sec, 2 times). Lysates were centrifuged at 14000 rpm for 15 min at 4 °C. In a new tube, 10 μL Tris (2-carboxyethyl)phosphine hydrochloride (10 mM) was added to 50 μL supernatant and, incubated for 15 min at room temperature. Next, 40 μL ammonium sulfate solution (0.6 M) was added, and samples were spun down. The clear supernatant (50 μL) was then derivatized with 45 μL SBD-F (ammonium 7-fluorobenzo-2-oxa-1,3-diazole-4-sulfonate; 1 mg/mL in borax buffer: 0.1 M containing 1 mM EDTA, pH 9.5) plus 5 μL ammonia solution (12.5% v/v), and incubated shaking at 500 rpm at 60 °C for 1 h (protect from light). Lastly, samples were spun down (14000 rpm, 15 min, 4 °C), and the supernatant was measured using the HPLC method (employing Phenomenex Gemini NX-C18 analytical column, 4.6 \times 150 mm; 3 μm particles) and fluorescence detection.

Table S2. List of human primer sequences used in RT-qPCR.

Gene Name	Forward and reverse primer sequence (5'- 3')
<i>PANK1</i>	Fwd: AGGTGTCAGCATTCTAGCCGTG Rev: GGTCTCACACCAGTCAGCAAG
<i>PANK2</i>	Fwd: CGTGGAGATAGCACCAAAGTGG Rev: CAGGTCCTCTTACTGACAGCC
<i>PANK3</i>	Fwd: TTGCCAGGTTGGGCTGTAGCAT Rev: GCACACATTCGTGCCACAGAAC
<i>PANK4</i>	Fwd: TCGTGGATTCTACAGCGAGTG Rev: CTGTCCCTCTAAGGAGTAGCTC
<i>PPCS</i>	Fwd: TCCTGGCAGTAGAGTTCACCAC Rev: GGCATTTTCAGAGACAGGAACATAG
<i>PPCDC</i>	Fwd: CAAGAAGCTGGTGTGCGGAGAT Rev: GTCAACTCTGCTGGAAGCCACT
<i>COASY</i>	Fwd: TGAGGTGTGGACTGCTGTCATC Rev: TGGCTCTGTTCCACAAGCTGCT
<i>SLC25A42</i>	Fwd: AGTTCAGCGCACACGAGGAGTA Rev: GTAGGTCAGTGAAGCGGCTGTC
<i>SLC25A16</i>	Fwd: ATGCTCCTACCCTTCTTGGCAG Rev: TTGCATTCGCCGACGAGTCACA
<i>SLC25A17</i>	Fwd: GGTGGTAAACACCAGACTGAAGC Rev: AGCCGAGATTCCTTCATCGCGA
<i>CPT1b</i>	Fwd: TGTATCGCCGTAACACTGGACCG Rev: TGTCTGAGAGGTGCTGTAGCAC
<i>CPT2</i>	Fwd: GCAGATGATGGTTGAGTGCTCC Rev: AGATGCCGACAGAGCAAACAAGTG
<i>CRAT</i>	Fwd: CCTACAGACCAACAAGGAGCCT Rev: TGCATCTAGGCACACGGTGAAG
<i>CROT</i>	Fwd: CTAGTGAGGAGCGAACTCGATG Rev: CCTCTGGTGTACATGTGGACTG
<i>ACOT1</i>	Fwd: GGGTTTTGCTGTGATGGCTCTG Rev: CAGCCCAACTCCTGGACCTTTT
<i>ACOT2</i>	Fwd: ATGGAGACGCTCCATCTGGAGT Rev: GTGATGCCCTTCAGGAAAGAGG
<i>ACOT4</i>	Fwd: CTTTGCCACGTTGGCTCTAGCT Rev: CCTAGAGAAATGCCAAAAGCCC
<i>ACOT6</i>	Fwd: GAGCAATCCACTGGAGGAACAC Rev: GAGCTTGTAGCCTTTCAGAGGC
<i>ACOT7</i>	Fwd: CTACACCTCCAAGCACTCTGTG Rev: CCTTGTCCACATTCTTCAGCGAC

<i>ACOT8</i>	Fwd: GCTGACCACTGGATGCTCTATG Rev: AGGTCACAGCTAGGACTCCATC
<i>ACOT9</i>	Fwd: ATCCACTCCGCCAAGATGTCTC Rev: GATGTCTTCCCGACCCAGCTAA
<i>ACOT11</i>	Fwd: TCTGGTGCTCAAAGCCATCGTG Rev: TCATCTGCGTCCAGGACCACAA
<i>ACOT12</i>	Fwd: GGAGGTTACCAGCACTGTGGAA Rev: GCCAAATGTGCTGGACTTCCCA
<i>ACOT13</i>	Fwd: CGGAGTCAGTGTGATATGAACA Rev: GCCTTGTTGGTCAGATCCACAG
<i>ABCD3</i>	Fwd: GTTCCTTTAGCAACGCCAAATGG Rev: CTCTTCCGCAGCCATTTGGAC
<i>NUDT7</i>	Fwd: CTCCGTCCTTTTGCCATTGGTG Rev: TGTCTGTAGGGTCACGCTTACC
<i>NUDT8</i>	Fwd: CTGGCAGTGCCCGAGGAGCA Rev: GCCTACACCAGCAAGCACTGG
<i>NUDT19</i>	Fwd: GCACCACTCGCCGCTTTGACA Rev: GTTGCCTCTGATGGAGATGACC
<i>YWHAZ</i>	Fwd: ACCGTTACTTGGCTGAGGTTGC Rev: CCCAGTCTGATAGGATGTGTTGG

Fwd, forward primer; Rev, reverse primer.

Table S3. List of murine primer sequences used in RT-qPCR.

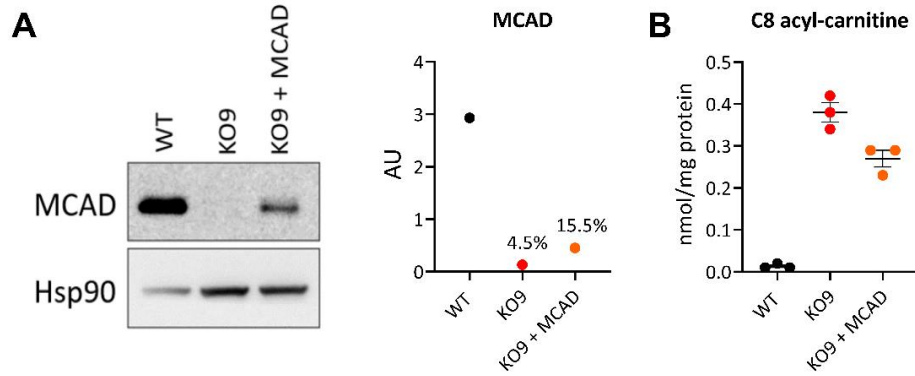
Gene Name	Forward and reverse primer sequence (5' - 3')
<i>Pank1a</i>	Fwd: GTTCGCCCAGCATGATTCTC Rev: CTTAACCAGGGTTCCACCGAT
<i>Pank1b</i>	Fwd: CTGAGCCTAACTCCATTCAACT Rev: TCCACCGATATCCATACCAAAC
<i>Pank2</i>	Fwd: TTGGGCATACGTGGAGCTTT Rev: TCTCACATACATTTCAACAGGACAAG
<i>Pank3</i>	Fwd: TCACTGGGAACCAAAGGATAAA Rev: CAGTGAGGGATACTTCCCATTATAG
<i>Pank4</i>	Fwd: GAAAACGGCCTCGCACTAAA Rev: CGCTCTTCCCAGCCTAGTGA
<i>Ppcs</i>	Fwd: CTCTCAGTCCATTAGGCTCTTC Rev: GGATCTTGTGTTTCAGGCATTTTC
<i>Ppcdc</i>	Fwd: TAACAACAGAGAGAGCCAAACA Rev: GCTTCCACATCTCCCATTCA
<i>Coasy</i>	Fwd: GGAGGCCTTTGGAACAGATATT Rev: GAGGATCTTCATCTGCTTCTTGT
<i>Cpt1a</i>	Fwd: CCATCCTGTCTGACAAGGTTTAG Rev: CCTCACTTCTGTTACAGCTAGCAC
<i>Cpt1b</i>	Fwd: GCACACCAGGCAGTAGCTTT Rev: CAGGAGTTGATTCCAGACAGGTA
<i>Cpt2</i>	Fwd: CAACTCGTATACCCAAACCCAGTC Rev: GTTCCATCTTGATCGAGGACATC
<i>Crat</i>	Fwd: GCTGCCAGAACCGTGGTAAA Rev: CCTTGAGGTAATAGTCCAGGGA
<i>Abcd1</i>	Fwd: GCTGTGACCTCCTACACTCTCC Rev: AGTAGTGCCAGTTCCACCTCA
<i>Abcd2</i>	Fwd: GAACTACCCCTCAGCGACAC Rev: ATGGCCTCTGTGGAATATAGAAC
<i>Acot1</i>	Fwd: AACATCACCTTTGGAGGGGAG Rev: TCCCAACCTCCAAACCATCA
<i>Acot2</i>	Fwd: AGTCAACGACGCAAAATGGTG Rev: GCTCTTCCAATCCTGTTGGC
<i>Acot3</i>	Fwd: GCTCAGTCACCCTCAGGTAA

Chapter 6

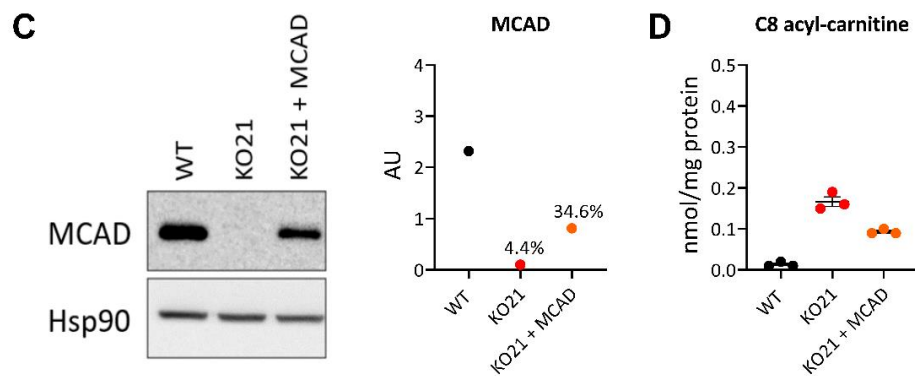
	Rev: AAGTTTCCGCCGATGTTGGA
<i>Acot4</i>	Fwd: ACATCCAAAGGTAAAAGGCCCA Rev: TCCACTGAATGCAGAGCCATT
<i>Acot6</i>	Fwd: ATCCTCAGGTGAAAGGCCCAA Rev: AAGGACAGTGGCTGTGATGTT
<i>Acot7</i>	Fwd: ATCAGCACGCGGCACTGTAA Rev: TTGGTACCTGTGAGGATGTTCTCC
<i>Acot8</i>	Fwd: AAGTATCGAGTGGGGCTGAAC Rev: TGATGTCACCTTCCCAATGT
<i>Acot9</i>	Fwd: GGGGCTTCTTACTCATGGCA Rev: CATGGTCTCTCCAGACTGTGG
<i>Acot11</i>	Fwd: GTGACCAGCGGCCCTTTAG Rev: AGAACATAGAGGCGAAGCCCCTT
<i>Acot12</i>	Fwd: CCGTGGCACTAAGGTCAGTT Rev: ACGTTACGGTGCACGAATTG
<i>Acot13</i>	Fwd: AGACTCTTGCTTTGCGTCCA Rev: GACAAGCGTCACCTTTTCCAA
<i>Nudt7</i>	Fwd: CCAAGTGGAGGTGGTCTCTC Rev: GATGAAATCACGGCCAGACT
<i>Nudt8</i>	Fwd: CAGTTTCCCAGGCGGTAAGT Rev: CACGTTGGCAAGTACTGGGA
<i>Nudt19</i>	Fwd: ATCTGTGCCATCCGCGAAGC Rev: CACAGCTGGAGGAAGCAGCG
<i>36b4</i>	Fwd: GGACCCGAGAAGACCTCCTT Rev: GCACATCACTCAGAATTTCAATGG

Fwd, forward primer; Rev, reverse primer.

WT vs MCAD KO9



WT vs MCAD KO21

**Figure S1. Partial MCAD reintroduction in MCAD-KO HepG2 cells partially restores phenotype.**

A. Representative immunoblot image and respective quantification of MCAD protein in WT, MCAD-KO clone KO9 cells, and KO cells overexpressing MCAD (KO9 + MCAD); HSP90 (heat shock protein) was used as loading control.; **B.** Intracellular level of C8-carnitine; n=3 technical replicates.; **C.** Representative immunoblot image and respective quantification of MCAD protein in WT, MCAD-KO clone KO21 cells, and KO cells overexpressing MCAD (KO21 + MCAD).; **D.** Intracellular level of C8-carnitine; n=3 technical replicates.

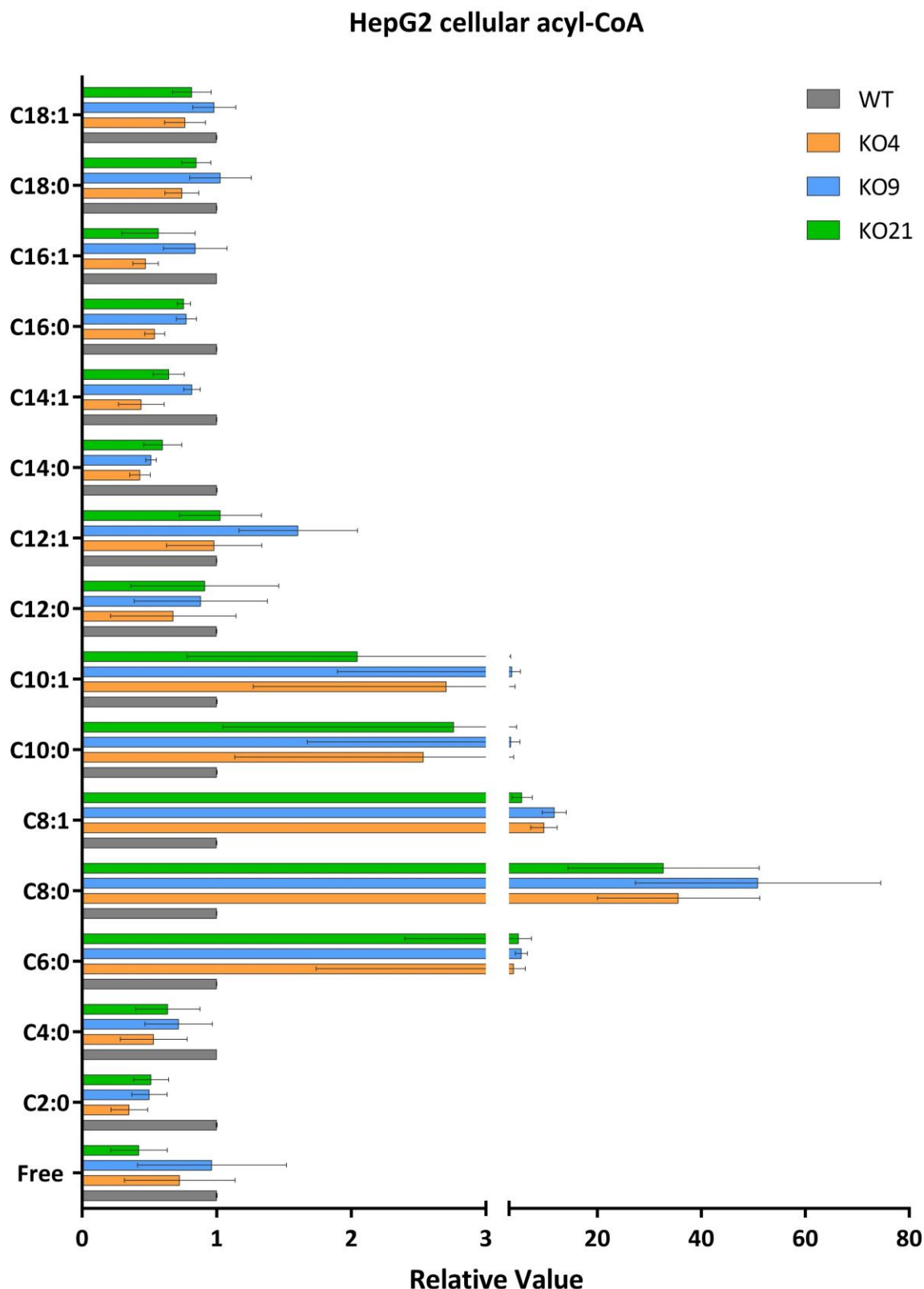


Figure S2. Full acyl-CoA profile in HepG2 cells incubated for 24 h in *high-fat no-glucose medium*. Values are relative to the mean WT value within each experiment. The data represents the average of independent experiments ($n=3$). Each independent experiment consisted of 4-5 technical replicates; \pm standard error of the mean (SEM). Each colour represents one cell line – one WT and three MCAD-KO (KO4, KO9 and KO21).

Table S4. Statistical significance of differences in acyl-CoA levels between MCAD-KO clones and WT incubated in *high-fat no-glucose medium*. One-way Brown-Forsythe ANOVA adjusted by Dunnett's T3 multiple comparisons test was performed per individual experiment (n=3) on the data displayed in **Figure S2**. N1, N2, N3 denote the number of independent experiments. Each independent experiment in turn consists of 4-5 technical replicates. * $p < 0.05$, ** $p < 0.01$, *** $p < 0.005$, **** $p < 0.001$. Orange cells indicate cases where the KO had a higher value relative to the WT, while blue cells indicate a lower value in KO relative to the WT. *Black highlighted cells represent cases where no measurements were obtained for a given species.*

MCAD-KO clones	KO4			KO9			KO21		
Acyl-CoAs	N1	N2	N3	N1	N2	N3	N1	N2	N3
Free		*			**		*	**	
C2:0	*	****	****		****	***		****	***
C4:0	**	**			**		*	**	
C6:0	*	***	****	**	****	***	***	****	**
C8:0	**	****	****	**	****	***	***	****	**
C8:1		*	**		**	**		**	**
C10:0		**	**		**	***		**	**
C10:1		*	**	*	*	*			*
C12:0	**			**			**		
C12:1					**				
C14:0	**	***		*	****		**	**	
C14:1	*	*					*		
C16:0	*	****			**			*	
C16:1	*	**			**			****	
C18:0		*							
C18:1		**						**	

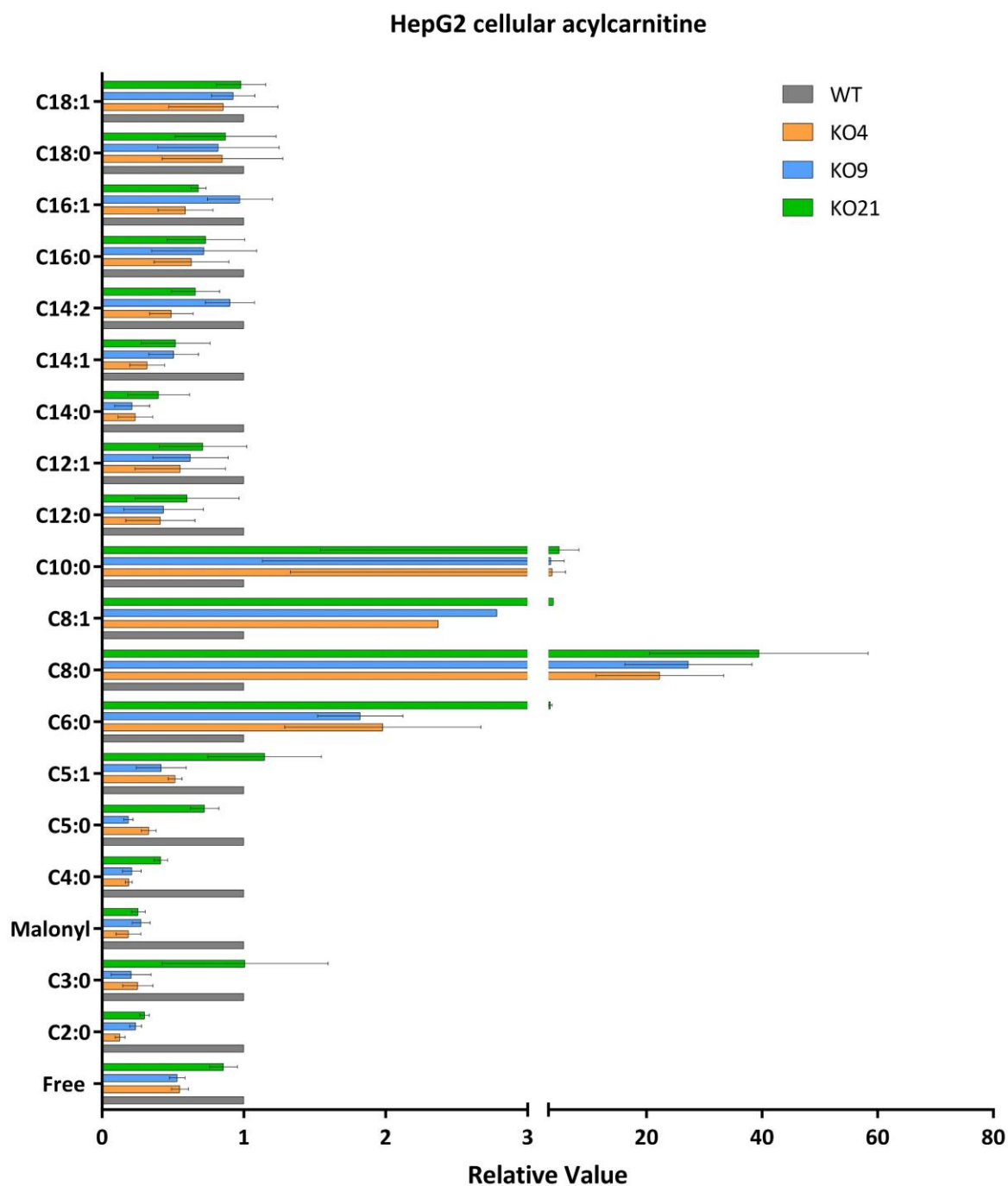


Figure S3. Full acylcarnitine profile in HepG2 cells incubated for 24 h in *high-fat no-glucose medium*. Values are relative to the mean WT value within each experiment. The data represents the average of independent experiments (n=3). Each independent experiment consisted of 4-5 technical replicates; \pm standard error of the mean (SEM). Each colour represents one cell line – one WT and three MCAD-KO (KO4, KO9, and KO21).

Table S5. Statistical significance of differences in acylcarnitine levels between MCAD-KO clones and WT incubated in *high-fat no-glucose medium*. One-way Brown-Forsythe ANOVA adjusted by Dunnett's T3 multiple comparisons test was performed per individual experiment (n=3) on the data displayed in **Figure S3**. N1, N2, N3 denote the number of independent experiments. Each independent experiment in turn consists of 4-5 technical replicates. * $p < 0.05$, ** $p < 0.01$, *** $p < 0.005$, **** $p < 0.001$. Orange cells indicate cases where the KO had a higher value relative to the WT, while blue cells indicate a lower value in KO relative to the WT. *Black highlighted cells represent cases where no measurements were obtained for a given species.*

MCAD-KO clones	KO4			KO9			KO21		
	N1	N2	N3	N1	N2	N3	N1	N2	N3
Free		**	****		*	****			
C2:0	**	****	****	**	****	****	*	****	****
C3:0	*	***	***	*	***	****	*	*	**
Malonyl	*	***	****		****	****	*	***	****
C4:0	**	***	****	*	***	****	*	**	****
C5:0	**	***	****	**	***	***		**	**
C5:1		***	***		***	****	*		
C6:0		**	***		****	***	***	****	****
C8:0	**	***	***	****	****	****	***	****	****
C8:1	**			***			****		
C10:0		****	****		****	****		****	****
C12:0	**	*	****	**	*	****	*		*
C12:1	*	*		*					
C14:0	****	***	****	****	***	****	****	***	***
C14:1	**	*	**	**	*		**		
C14:2	*	*					*		
C16:0	**	**	*	**			**		
C16:1	**		*				*	*	*
C18:0	**		**	***			**		*
C18:1	****			*					

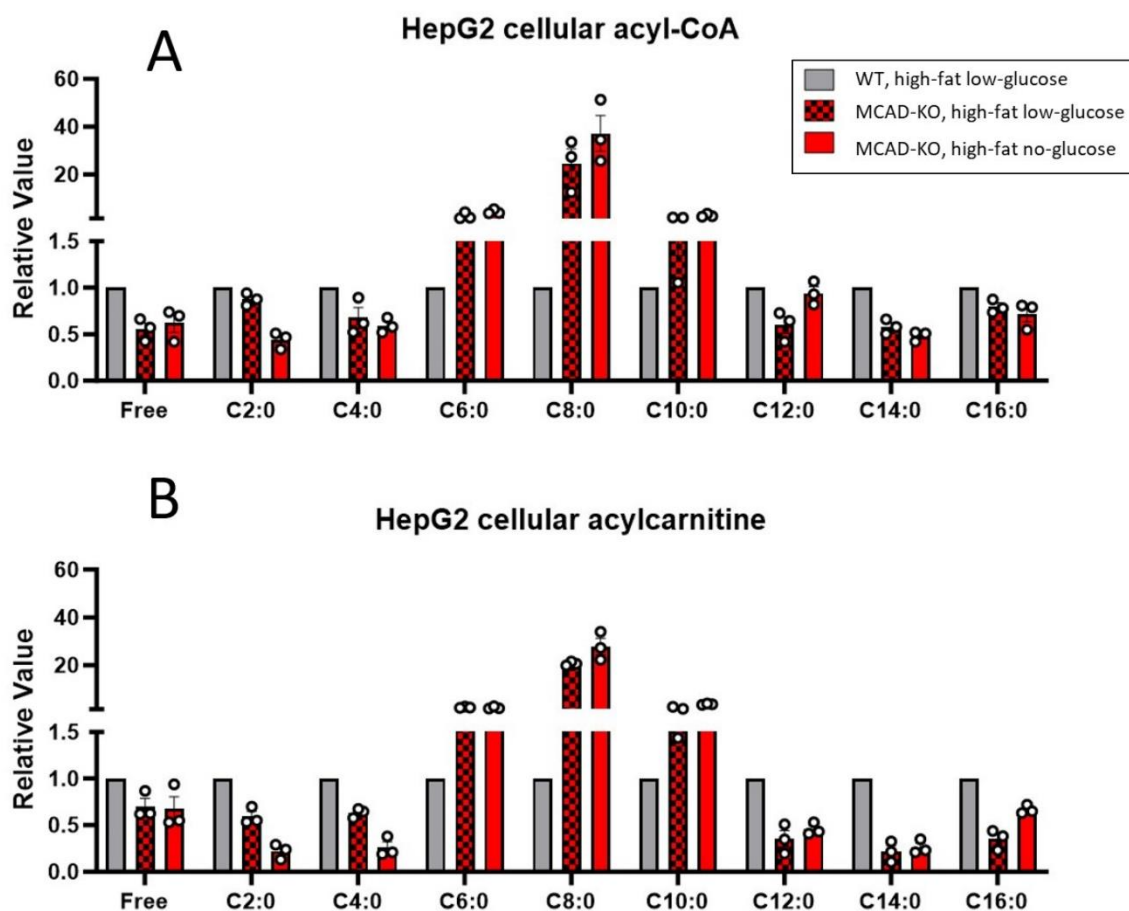


Figure S4. Acyl-CoA and acylcarnitine profiles of WT and MCAD-KO HepG2 cells grown under two conditions. Representative acyl-CoA and acylcarnitine accumulations in MCAD-KO relative to WT in HepG2 cells. Three KO-clones (KO4, KO9, KO21) and one WT cell line were investigated experimentally. Individual data points indicate the mean results for one cell line. The results consist of independent experiments (n=3) and technical replicates (n=4-5). The median and range are shown by the bar (error) bars. **A.** Acyl-CoA.; **B.** Acylcarnitines.

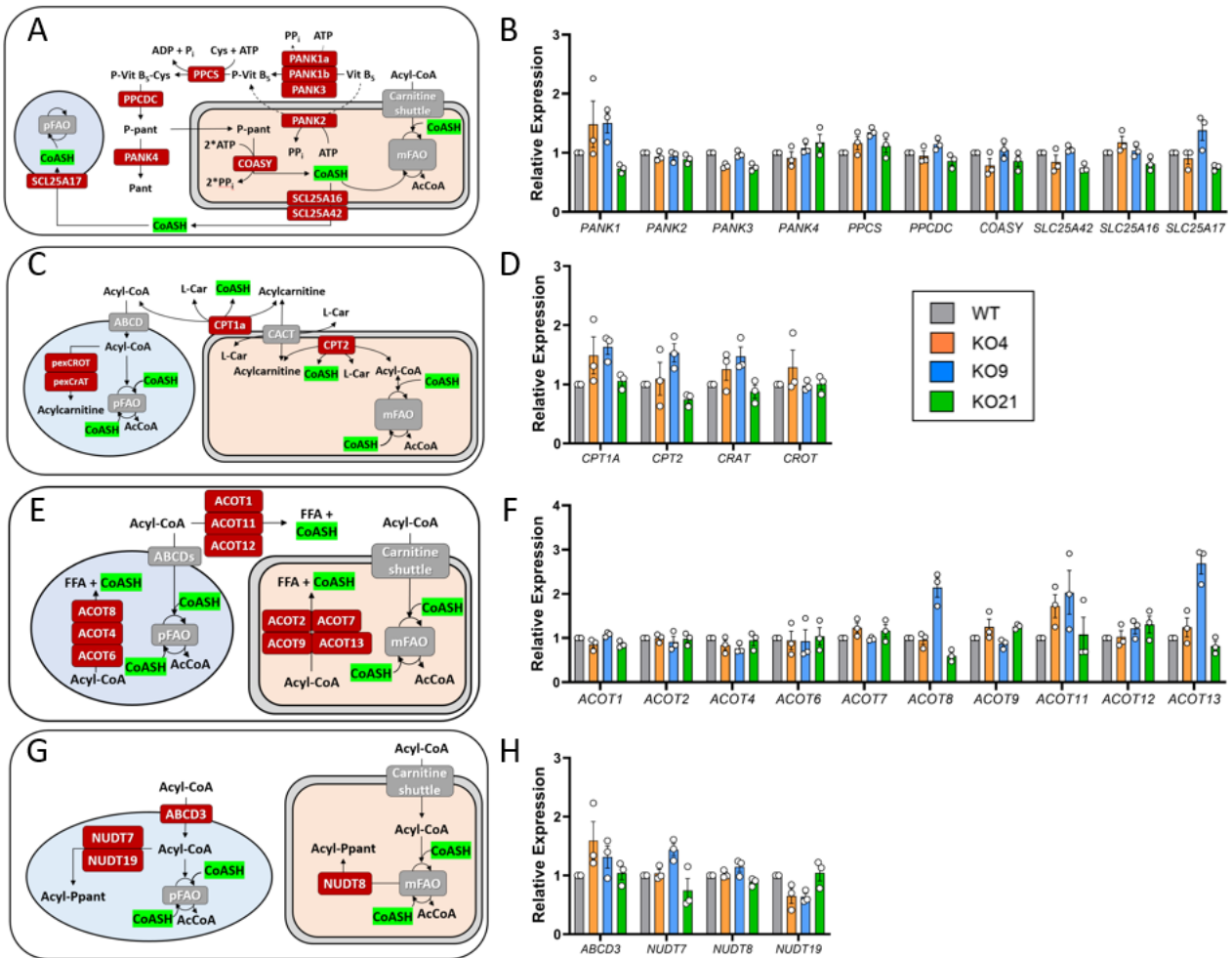


Figure S5. Gene expression data from MCAD-KO HepG2 cells in *high-fat no-glucose medium*. Relative expression of genes (relative to WT) in various pathways of CoA metabolism. Schemes of the relevant reactions are provided for clarity with three compartments: cytosol in white, mitochondria in pink, and peroxisomes in light blue. AcCoA = acetyl-CoA. **A & B.** CoA biosynthesis and transport. *PANK* = pantothenate kinase, *PPCS* = phosphopantothenate-cysteine ligase, *PPCDC* = phosphopantothenoylcysteine decarboxylase, *COASY* = bifunctional coenzyme A synthase, Vit B₅ = pantothenate, P-Vit B₅ = phosphopantothenate, P-Vit B₅-Cys = phosphopantothenoyl-cysteine, P-pant = phosphopantetheine, Pant = pantetheine, *SLC25A* = solute carrier family protein 25A.; **C & D.** Carnitine acyltransferases. *CPT* = carnitine palmitoyltransferase, *CRAT* = carnitine acetyltransferase, *CROT* = peroxisomal carnitine octanoyltransferase.; **E & F.** *ACOT* = Acyl-CoA thioesterases.; **G & H.** *ABCD3* = ATP-binding cassette domain protein 3, *NUDT* = nudix hydrolase. Expression values are relative to control WT (= 1); each data point represents the average of an independent experiment (3 experiments), which consisted of 4-5 technical replicates (cell cultures); ± standard error of the mean (SEM).

Table S6. Statistical significance of differences in mRNA expression between MCAD-KO clones and WT HepG2 cells incubated in *high-fat no-glucose medium*. One-way Brown-Forsythe ANOVA adjusted by Dunnett's T3 multiple comparisons test was performed per individual experiment (n=3) on the data displayed in **Figure S5**. These were therefore values relative to the WT mean within each experiment. Each experiment consisted of 4-5 technical replicates. Values were considered statistically significant when * $p < 0.05$. Highlighted in orange are upregulated genes in KO relative to WT while in blue are downregulated genes in KO relative to WT.

MCAD-KO clones	KO4			KO9			KO21		
	N1	N2	N3	N1	N2	N3	N1	N2	N3
<i>ACOT1</i>		*						*	
<i>ACOT2</i>		*			*			*	*
<i>ACOT4</i>				*					
<i>ACOT6</i>		*			*				
<i>ACOT7</i>	*		*				*		
<i>ACOT8</i>				*	*	*	*	*	*
<i>ACOT9</i>	*			*				*	
<i>ACOT11</i>	*	*		*	*	*	*	*	*
<i>ACOT12</i>									
<i>ACOT13</i>			*	*	*	*		*	
<i>NUDT7</i>				*	*			*	*
<i>NUDT8</i>				*					*
<i>NUDT19</i>	*	*	*	*	*	*	*	*	
<i>SLC25A42</i>	*	*					*	*	
<i>SLC25A16</i>			*						*
<i>SLC25A17</i>	*				*	*	*	*	*
<i>CRAT</i>		*	*	*	*	*		*	
<i>CROT</i>			*				*		
<i>CPT1A</i>		*	*	*	*	*		*	
<i>CPT2</i>	*		*		*	*			*
<i>PANK1</i>		*	*	*				*	*
<i>PANK2</i>									
<i>PANK3</i>	*	*	*				*	*	*
<i>PANK4</i>		*	*				*		
<i>PPCS</i>	*			*	*	*	*	*	
<i>PPCDC</i>						*	*		
<i>COASY</i>	*	*		*			*		
<i>ABCD3</i>			*	*					

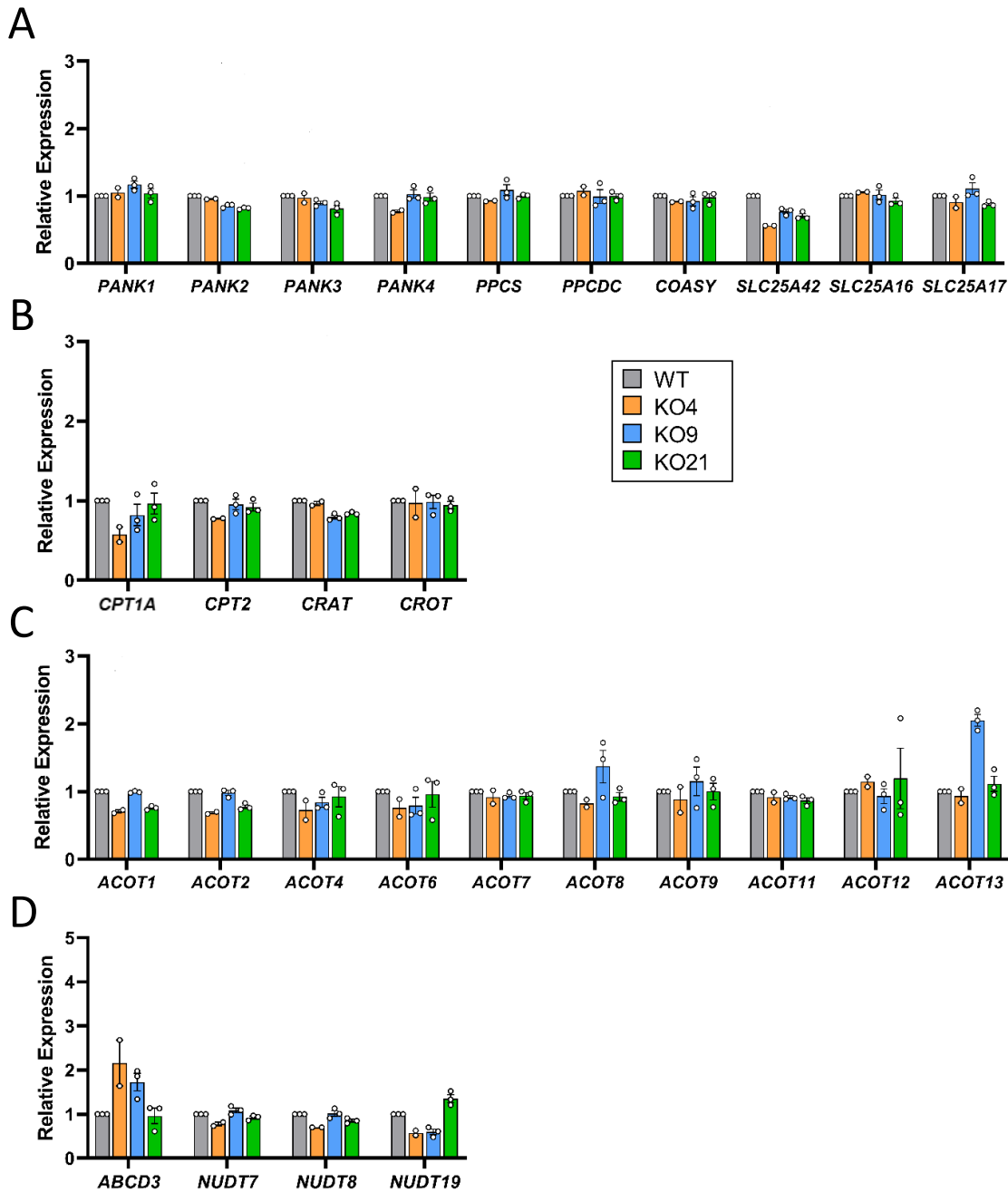


Figure S6. Gene expression data from MCAD-KO HepG2 cells in high-fat low-glucose medium. Relative expression of genes (relative to WT) in various pathways of CoA metabolism. **A**. CoA biosynthesis and transport. *PANK* = pantothenate kinase, *PPCS* = phosphopantothenate-cysteine ligase, *PPCDC* = phosphopantothenoylcysteine decarboxylase, *COASY* = bifunctional coenzyme A synthase, *SLC25A* = solute carrier family protein 25A.; **B**. Carnitine acyltransferases. *CPT* = carnitine palmitoyltransferase, *CRAT* = carnitine acetyltransferase, *CROT* = peroxisomal carnitine octanoyltransferase.; **C**. *ACOT* = Acyl-CoA thioesterases.; **D**. *ABCD* = ATP-binding cassette domain protein, *NUDT* = nudix hydrolase. Expression values are relative to control WT (= 1); each data point represents the average of an independent experiment (3 experiments), which consisted of 4-5 technical replicates (cell cultures); \pm standard error of the mean (SEM).

Table S7. Statistical significance of differences in mRNA expression between MCAD-KO clones and WT HepG2 cells incubated in *high-fat low-glucose medium*. One-way Brown-Forsythe ANOVA adjusted by Dunnett's T3 multiple comparisons test was performed per individual experiment (n=3) on the data displayed in **Figure S6**. These were therefore values relative to the WT mean within each experiment. Each experiment consisted of 4-5 technical replicates. Values were considered statistically significant when $* p < 0.05$. Highlighted in orange are upregulated genes in KO relative to WT while in blue are downregulated genes in KO relative to WT. *Experiment N3 in KO4 had technical issues due to which we were not able to perform the gene expression analysis.*

MCAD-KO clones	KO4			KO9			KO21		
Gene of Interest	N1	N2	N3	N1	N2	N3	N1	N2	N3
<i>ACOT1</i>	*								*
<i>ACOT2</i>	*	*						*	*
<i>ACOT4</i>		*							
<i>ACOT6</i>									*
<i>ACOT7</i>									
<i>ACOT8</i>	*	*		*	*	*			
<i>ACOT9</i>				*	*				*
<i>ACOT11</i>									
<i>ACOT12</i>								*	
<i>ACOT13</i>	*			*	*	*			*
<i>NUDT7</i>	*								
<i>NUDT8</i>		*							*
<i>NUDT19</i>	*	*		*	*	*	*	*	*
<i>SLC25A42</i>	*	*		*		*	*	*	*
<i>SLC25A16</i>									*
<i>SLC25A17</i>						*			*
<i>CRAT</i>				*	*	*	*	*	*
<i>CROT</i>	*								
<i>CPT1A</i>	*	*		*	*		*		
<i>CPT2</i>	*	*			*			*	
<i>PANK1</i>				*					
<i>PANK2</i>							*	*	*
<i>PANK3</i>							*	*	*
<i>PANK4</i>		*				*			
<i>PPCS</i>						*			
<i>PPCDC</i>									
<i>COASY</i>									*
<i>ABCD3</i>		*			*				*